Cell Reports

Article

# The glutathione peroxidase Gpx4 prevents lipid peroxidation and ferroptosis to sustain Treg cell activation and suppression of antitumor immunity

## Graphical abstract

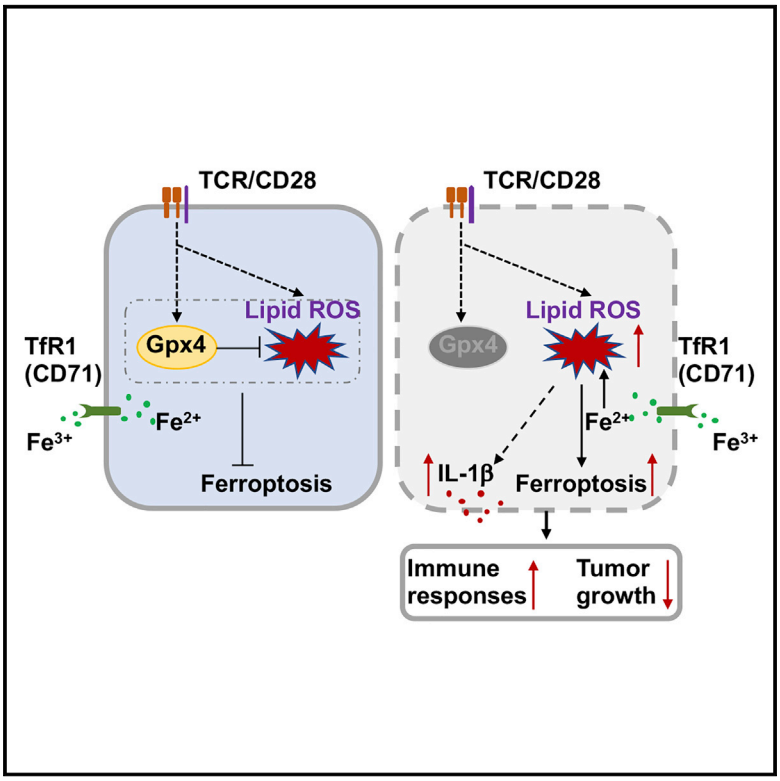


## Authors

Chengxian Xu, Shaogang Sun, Travis Johnson, Rong Qi, Siyuan Zhang, Jie Zhang, Kai Yang

## Correspondence

ky11@iu.edu

## In brief

Actively maintaining cellular redox homeostasis is crucial to sustain Treg activation and function. Xu et al. demonstrate that Gpx4 serves as a metabolic checkpoint in protecting activated Treg cells from uncontrolled lipid peroxidation and ferroptosis. Moreover, deletion of Gpx4 in Treg cells impedes tumor immune evasion without inducing overt autoimmunity.

## Highlights

- Treg cells need Gpx4 to maintain immune tolerance but not their survival at steady state
- Gpx4 prevents lipid peroxidation and ferroptosis to sustain Treg cell activation
- IL-1β derived from ferroptotic Treg cells lacking Gpx4 facilitates $T_H17$ responses
- Gpx4 promotes survival of intratumoral Treg cells to repress antitumor immunity

Xu et al., 2021, Cell Reports *35*, 109235
June 15, 2021 
https://doi.org/10.1016/j.celrep.2021.109235

CellPress

Cell Reports

CellPress
OPEN ACCESS

Article

# The glutathione peroxidase Gpx4 prevents lipid peroxidation and ferroptosis to sustain Treg cell activation and suppression of antitumor immunity

Chengxian Xu,[1] Shaogang Sun,[1] Travis Johnson,[2] Rong Qi,[3] Siyuan Zhang,[4,5] Jie Zhang,[6] and Kai Yang[1,5,7,8,*]

[1]Department of Pediatrics and the Herman B Wells Center for Pediatric Research, Indiana University School of Medicine, Indianapolis, IN 46202, USA
[2]Department of Biostatistics, Indiana University School of Medicine, Indianapolis, IN 46202, USA
[3]Indiana Biosciences Research Institute, Indianapolis, IN 46202, USA
[4]Department of Biological Sciences, College of Science, University of Notre Dame, Notre Dame, IN 46556, USA
[5]Melvin and Bren Simon Comprehensive Cancer Center, Indiana University School of Medicine, Indianapolis, IN 46202, USA
[6]Department of Medical and Molecular Genetics, Indiana University School of Medicine, Indianapolis, IN 46202, USA
[7]Department of Microbiology and Immunology, Indiana University School of Medicine, Indianapolis, IN 46202, USA
[8]Lead contact
*Correspondence: ky11@iu.edu
https://doi.org/10.1016/j.celrep.2021.109235

## SUMMARY

T regulatory (Treg) cells are crucial to maintain immune tolerance and repress antitumor immunity, but the mechanisms governing their cellular redox homeostasis remain elusive. We report that glutathione peroxidase 4 (Gpx4) prevents Treg cells from lipid peroxidation and ferroptosis in regulating immune homeostasis and antitumor immunity. Treg-specific deletion of Gpx4 impairs immune homeostasis without substantially affecting survival of Treg cells at steady state. Loss of Gpx4 results in excessive accumulation of lipid peroxides and ferroptosis of Treg cells upon T cell receptor (TCR)/CD28 co-stimulation. Neutralization of lipid peroxides and blockade of iron availability rescue ferroptosis of Gpx4-deficient Treg cells. Moreover, Gpx4-deficient Treg cells elevate generation of mitochondrial superoxide and production of interleukin-1β (IL-1β) that facilitates T helper 17 ($T_H17$) responses. Furthermore, Treg-specific ablation of Gpx4 represses tumor growth and concomitantly potentiates antitumor immunity. Our studies establish a crucial role for Gpx4 in protecting activated Treg cells from lipid peroxidation and ferroptosis and offer a potential therapeutic strategy to improve cancer treatment.

## INTRODUCTION

T regulatory (Treg) cells expressing the lineage transcription factor Foxp3 play pivotal roles in regulating immune tolerance and antitumor immune responses (Plitas and Rudensky, 2016). Treg cells in the periphery are classified into thymus-derived Treg (tTreg) cells and peripherally derived Treg (pTreg) cells with different suppressive capacities and functional stabilities (Josefowicz et al., 2012). Microenvironmental cues including antigen and cytokine milieu drive Treg cell activation and differentiation into various effector Treg subsets to repress distinct T cell responses (Canli et al., 2016; Newton et al., 2016). Treg cells obtain an ability to resist cell death induced by high oxidative stress frequently existing in the tumor microenvironment (TME) (Mougiakakos et al., 2009, 2011). Clinical evidence indicates that elevated proportions of intratumoral Treg cells often correlate with poor prognosis and low survival rates in various cancer patients (Nishikawa and Sakaguchi, 2014; Speiser et al., 2016). Therapeutic suppression of Treg cell survival in the TME has been emerging as an attractive strategy to potentiate antitumor immunity (Togashi et al., 2019). However, a recent study shows that apoptotic Treg cells induced by high oxidative stress in the TME exhibit enhanced immunosuppressive function and consequently facilitate tumor growth (Maj et al., 2017). Thus, a better understanding of regulatory mechanisms underpinning Treg cell survival may benefit the development of novel strategies to modulate Treg suppression of antitumor immunity.

Glutathione peroxidase 4 (Gpx4) is a selenoenzyme that reduces membrane phospholipid hydroperoxides to maintain cellular redox homeostasis using glutathione (GSH) as a cofactor (Seiler et al., 2008). Inactivation or depletion of Gpx4 in a variety of cell types can induce ferroptosis (Yang et al., 2014; Yang and Stockwell, 2008), which is a non-apoptotic form of cell death resulting from accumulation of toxic lipid peroxides with a reliance on ferrous iron (Stockwell et al., 2017). Neutralization of cellular lipid peroxides and blockade of iron availability represent well-established strategies to prevent ferroptotic cell death (Dixon et al., 2012; Yang et al., 2014). Extensive studies have focused on understanding the induction and regulation of ferroptosis in cancer and neurodegeneration (Chen et al., 2015; Chu et al.,

2019; Doll et al., 2017; Gao et al., 2019; Hambright et al., 2017; Kagan et al., 2017; Liu and Wang, 2019; Stockwell et al., 2017), whereas little is known about the role of Gpx4 and ferroptosis in regulating T cell homeostasis and immune responses (Matsushita et al., 2015). Despite the notion that conventional T cells lacking Gpx4 fail to maintain their homeostasis and mount protective immunity against bacterial infection, Gpx4-deficient Treg cells retain intact homeostatic survival and expansion (Matsushita et al., 2015). Compared to resting Treg cells under steady state, antigen-stimulated Treg cells markedly reprogram lipid synthesis and fatty acid oxidation in support of their expansion and function (Field et al., 2020; Michalek et al., 2011), which potentially enhance generation of lipid peroxides. Whether Gpx4 is required to regulate activation and accumulation of lipid peroxides in Treg cells remains to be established.

In this study, we establish an intrinsic role for Gpx4 in preventing Treg cell lipid peroxidation and ferroptosis in immune tolerance and antitumor immunity. We found that Gpx4 was dispensable to maintain Treg cell homeostasis in lymphoid and non-lymphoid tissues, whereas promoting suppression of T helper 1 ($T_H1$) and $T_H17$ responses at steady state. In response to T cell receptor (TCR) and co-stimulatory signals, Gpx4-deficient Treg cells displayed aberrant accumulation of cellular lipid peroxides and underwent ferroptosis. Moreover, loss of Gpx4 disrupted mitochondrial fitness of Treg cells and enhanced their interleukin-1β (IL-1β) production, which promoted $T_H17$ responses. Furthermore, Treg-specific deletion of Gpx4 compromised survival of intratumoral Treg cells and potentiated antitumor immune responses leading to enhanced tumor regression. Our results highlight that Treg cells need Gpx4 to neutralize lipid peroxides and prevent ferroptosis to sustain Treg cell activation and function in maintaining immune homeostasis and restraining antitumor immunity.

## RESULTS

### Treg-specific deletion of Gpx4 promotes $T_H17$ responses

To define the physiological relevance of Gpx4 in Treg cells, we crossed mice carrying *loxP*-flanked *Gpx4* alleles (*Gpx4*$^{fl/fl}$) (Yoo et al., 2012) with *Foxp3*$^{YFP\text{-}Cre}$ (*Foxp3*$^{Cre}$) (Rubtsov et al., 2008) mice (denoted hereafter as *Foxp3*$^{Cre}$*Gpx4*$^{fl/fl}$ mice) to specifically delete Gpx4 in Treg cells. Quantitative PCR and western blot results showed that Gpx4 was efficiently deleted at both mRNA and protein levels in Treg cells (Figures S1A and S1B). We next examined whether Gpx4 deficiency affects Treg-dependent maintenance of immune homeostasis. Compared to WT littermates, *Foxp3*$^{Cre}$*Gpx4*$^{fl/fl}$ mice showed normal frequencies and numbers of naive (CD62L$^{hi}$CD44$^{lo}$) and effector/memory (CD44$^{hi}$CD62L$^{lo}$) populations in both CD4$^+$ and CD8$^+$ T cells (Figure 1A) as well as center memory (CD62L$^{hi}$CD44$^{hi}$) CD8$^+$ T cells (Figure 1A). To characterize features of T cell responses, we examined cytokine production by conventional CD4$^+$ and CD8$^+$ T cells from WT and *Foxp3*$^{Cre}$*Gpx4*$^{fl/fl}$ mice. The proportions of interferon-γ (IFN-γ)- and IL-4-producing CD4$^+$ T cells (Figure 1B) and IFN-γ-producing CD8$^+$ T cells (Figure 1C) were comparable between WT and *Foxp3*$^{Cre}$*Gpx4*$^{fl/fl}$ mice (approximately 8 weeks old). However, *Foxp3*$^{Cre}$*Gpx4*$^{fl/fl}$ mice showed a small but significant increase of IL-17-producing CD4$^+$ T cells (Figure 1D). In line with the requirement of Treg cells for maintaining immune homeostasis over a lifetime, *Foxp3*$^{Cre}$ *Gpx4*$^{fl/fl}$ mice at or above 6 months of age showed more profound increase of IL-17-producing CD4$^+$ T cells (Figure 1E), associated with elevated proportions of splenic neutrophils (Figure 1F), whereas retaining comparable proportions of IL-4- (Figure S1C) and IFN-γ- (Figure S1D) producing CD4$^+$ T cells and IFN-γ-producing CD8$^+$ T cells (Figure S1E). Collectively, mice with Treg-specific deletion of Gpx4 display an aberrant $T_H17$ disorder at steady state.

### Gpx4 differentially regulates Treg cell homeostasis in lymphoid and non-lymphoid tissues

Appropriate maintenance of Treg cell homeostasis is crucial to maintain immune tolerance. We thus assessed the impact of Gpx4 deficiency on Treg cells in lymphoid and non-lymphoid organs. WT and *Foxp3*$^{Cre}$*Gpx4*$^{fl/fl}$ mice had comparable proportions and numbers of splenic Treg cells (Figure 2A), which were apparently normal in *Foxp3*$^{Cre}$*Gpx4*$^{fl/fl}$ mice at or above 6 months of age (Figure S2A). Treg cells can be divided into resting (CD62L$^{hi}$CD44$^{lo}$) and effector (CD62L$^{lo}$CD44$^{hi}$) subsets, which display differential localization and function at steady state (Smigiel et al., 2014). Loss of Gpx4 did not substantially affect proportions of the Treg subsets (Figure S2B), indicating that Gpx4 is dispensable for splenic Treg cell homeostasis. We next examined expression of key Treg markers on Gpx4-deficient Treg cells. The expression of the Treg lineage transcription factor Foxp3 (Figure 2B) and Treg effector molecules including CTLA4 (Figure 2C), CD73, PD1, and NRP1 (Figures S2C–S2E) was comparable between WT and Gpx4-deficient Treg cells. Collectively, Gpx4 is dispensable to maintain Treg cell homeostasis in lymphoid tissues.

Treg cells at barrier surfaces, including lung, liver, and colon, are crucial to prevent unwanted T cell responses to harmless antigens (Panduro et al., 2016). We found that *Foxp3*$^{Cre}$*Gpx4*$^{fl/fl}$ mice had reduced frequencies of Treg cells in the liver and colon (Figure 2D) but normal frequencies of lung Treg cells (Figure 2D). However, the numbers of Treg cells in those tissues were comparable between WT and *Foxp3*$^{Cre}$*Gpx4*$^{fl/fl}$ mice (Figure 2D). These findings prompted us to examine whether loss of Gpx4 impairs Treg cell function in suppressing T cell responses in the liver and colon. Compared to WT mice, *Foxp3*$^{Cre}$*Gpx4*$^{fl/fl}$ mice exhibited markedly increased proportions of IL-17-producing CD4$^+$ T cells (Figure 2E) and IFN-γ-producing CD8$^+$ T cells (Figure 2F) in the colon. In line with this observation, *Foxp3*$^{Cre}$*Gpx4*$^{fl/fl}$ mice exhibited notable inflammation in the colon (Figure S2F). In contrast, the proportions of liver IL-17-producing CD4$^+$ T cells (Figure S2G) and IFN-γ-producing CD8$^+$ T cells (Figure S2H) were largely normal in *Foxp3*$^{Cre}$*Gpx4*$^{fl/fl}$ mice. Collectively, these results suggest that Gpx4 regulates Treg cell homeostasis and function in a tissue-context-dependent manner.

### Gpx4 protects activated Treg cells from aberrant lipid peroxidation and ferroptosis

TCR and co-stimulatory signals drive Treg cell activation, differentiation, and function in regulating immune tolerance and

CellPress
OPEN ACCESS

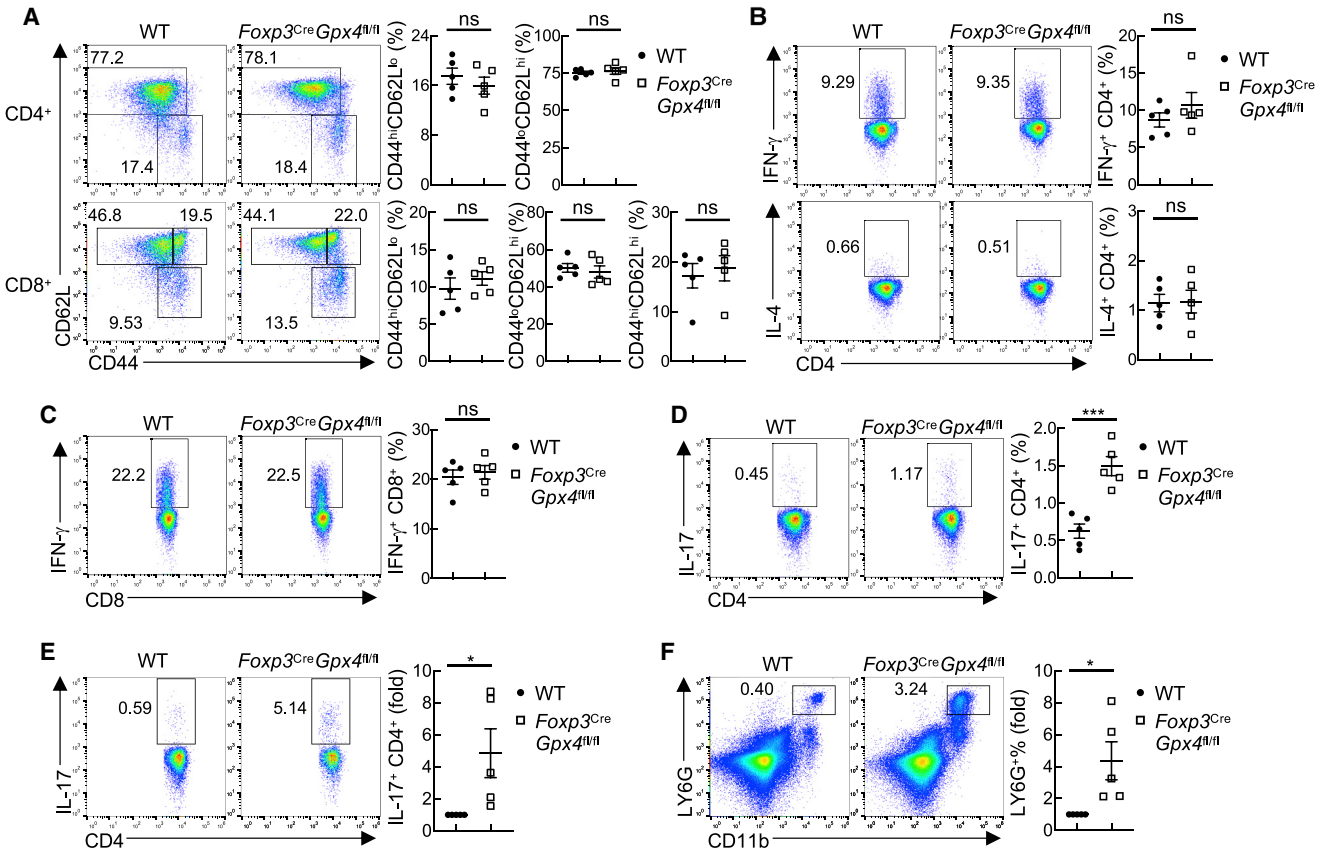


**Figure 1. *Foxp3*$^{Cre}$*Gpx4*$^{fl/fl}$ mice exhibit increased $T_H17$ responses**

(A) Expression of CD62L and CD44 on splenic conventional CD4$^+$ and CD8$^+$ T cells from 8-week-old WT and *Foxp3*$^{Cre}$*Gpx4*$^{fl/fl}$ mice. Right: proportions of effector (CD44$^{hi}$CD62L$^{lo}$) cells, resting (CD62L$^{hi}$CD44$^{lo}$) CD4$^+$ and CD8$^+$ cells, or memory (CD44$^{hi}$CD62L$^{hi}$) CD8$^+$ T cells (n = 5 each group).

(B) Expression of IFN-γ and IL-4 in splenic CD4$^+$ T cells from 8-week-old WT and *Foxp3*$^{Cre}$*Gpx4*$^{fl/fl}$ mice (n = 5 each group). Right: proportions of IFN-γ- or IL-4-producing CD4$^+$ T cells.

(C) Expression of IFN-γ in splenic CD8$^+$ T cells from 8-week-old WT and *Foxp3*$^{Cre}$*Gpx4*$^{fl/fl}$ mice (n = 5 each group). Right: proportions of IFN-γ-producing CD8$^+$ T cells.

(D) Expression of IL-17 in splenic CD4$^+$ T cells from 8-week-old WT and *Foxp3*$^{Cre}$*Gpx4*$^{fl/fl}$ mice (n = 5 each group). Right: proportions of IL-17-producing CD4$^+$ T cells.

(E) Expression of IL-17 in splenic CD4$^+$ T cells from 7-month-old WT and *Foxp3*$^{Cre}$*Gpx4*$^{fl/fl}$ mice (n = 5 each group). Right: fold changes of IL-17-producing CD4$^+$ T cells.

(F) Flow cytometry analysis of splenic neutrophils (CD11b$^+$LY6G$^+$) from 7-month-old WT and *Foxp3*$^{Cre}$*Gpx4*$^{fl/fl}$ mice. Right: fold changes of neutrophils (n = 5 each group).

Data are representative of at least three independent experiments. Data are mean ± SEM. The p values are determined by two-tailed Student's t test. *p < 0.05, ***p < 0.001. ns, not significant. Numbers in gates indicate the percentage of cells.

inflammatory responses (Canli et al., 2016). We noted that Treg cells rapidly induced expression of *Gpx4* at 2 h post anti-CD3 and anti-CD28 (α-CD3-CD28) stimulation (Figure S3A), followed by gradual downregulation (Figure S3A). To determine the role of Gpx4 in activated Treg cells, we first treated WT Treg cells with RSL3, a potent and selective inhibitor of Gpx4 (Yang et al., 2014), in the presence of α-CD3-CD28 stimulation. The extent of lipid peroxides in Treg cells was assessed by a well-established lipophilic reactive oxygen species (ROS) sensor, C11-BODIPY (Dixon et al., 2012). RSL3 notably elevated levels of C11-BODIPY (Figure 3A) and compromised viability of activated Treg cells (Figure 3B). Second, we treated WT and Gpx4-deficient Treg cells with α-CD3-CD28 and assessed their survival and lipid peroxidation with Liperfluo, a specific indicator of lipid peroxides (Dixon et al., 2012). Gpx4-deficient Treg cells displayed marked accumulation of lipid peroxides upon TCR/CD28 co-stimulation (Figure 3C), concomitant with disrupted viability (Figure 3D). Collectively, Gpx4 is crucial to prevent activated Treg cells from excessive lipid peroxidation and ferroptosis.

GSH represents the major non-enzymatic antioxidant that suppresses ferroptotic cell death of cancer cells (Yang et al., 2014). We determined the effect of GSH on ferroptosis of activated Gpx4-deficient Treg cells. Unexpectedly, supplementation of GSH failed to rescue ferroptosis of Gpx4-deficient Treg cells (Figure 3E). To examine the extent to which reduction of cellular GSH induces Treg cell ferroptosis, we treated Treg cells

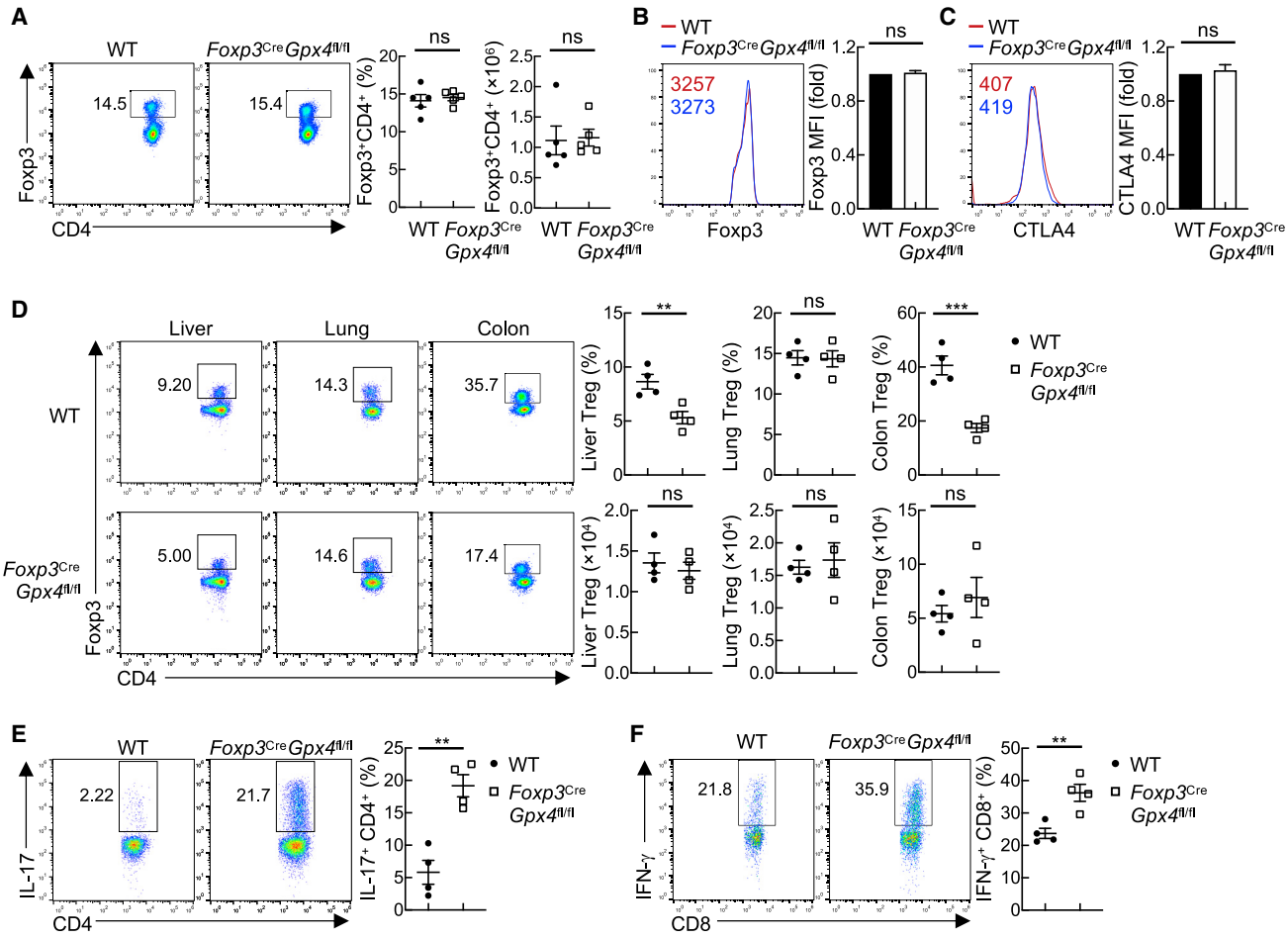


**Figure 2. Gpx4 is differentially required for Treg cell homeostasis in lymphoid and non-lymphoid tissues**

(A) Flow cytometry analysis of splenic Treg cells from 8-week-old WT and *Foxp3*$^{Cre}$*Gpx4*$^{fl/fl}$ mice. Percentage (middle) and numbers (right) of splenic Treg cells (n = 5 each group).

(B) Expression of Foxp3 in splenic Treg cells from 8-week-old WT and *Foxp3*$^{Cre}$*Gpx4*$^{fl/fl}$ mice. Numbers in graphs indicate mean fluorescence intensity (MFI) of Foxp3. Right: fold changes of Foxp3 MFI in splenic Treg cells (n = 5 each group).

(C) Expression of CTLA4 on splenic Treg cells from 8-week-old WT and *Foxp3*$^{Cre}$*Gpx4*$^{fl/fl}$ mice. Numbers in graphs indicate CTLA4 MFI. Right: fold changes of CTLA4 MFI on splenic Treg cells (n = 5 each group).

(D) Flow cytometry analysis of Treg cells in the liver, lung, and colon from 8-week-old WT and *Foxp3*$^{Cre}$*Gpx4*$^{fl/fl}$ mice. Right: percentage and numbers of Treg cells (n = 4 each group).

(E) Expression of IL-17 in colonic CD4$^+$ T cells from 8-week-old WT and *Foxp3*$^{Cre}$*Gpx4*$^{fl/fl}$ mice (n = 4 each group). Right: proportions of IL-17-producing CD4$^+$ T cells.

(F) Expression of IFN-γ in colonic CD4$^+$ T cells from 8-week-old WT and *Foxp3*$^{Cre}$*Gpx4*$^{fl/fl}$ mice (n = 4 each group). Right: proportions of IFN-γ-producing CD8$^+$ T cells.

Data are representative of at least three independent experiments. Data are mean ± SEM. The p values are determined by two-tailed Student's t test. **p < 0.01, ***p < 0.001. ns, not significant. Numbers in gates indicate the percentage of cells.

with erastin (a specific inhibitor of the cystine/glutamate antiporter; xCT) or buthionine sulfoximine (BSO; a specific inhibitor of the γ-glutamyl-cysteine synthetase; γ-GCS), which suppress biosynthesis of cellular GSH and induce ferroptosis (Yang et al., 2014). Both erastin and BSO rarely impaired Treg cell viability (Figures S3B and S3C), whereas triggering ferroptotic cell death of B16.F10 melanoma cells (Figure S3D). To explore whether loss of Gpx4 triggers other types of cell death accompanied by inducing ferroptosis, WT and Gpx4-deficient Treg cells were treated with Z-VAD-FMK (Z-VAD), necrostatin-1 (Nec-1) and necrostatin 2 racemate (Nec-1 s), and caspase-1 inhibitor (Casp1i), which inhibit apoptosis, necroptosis, and pyroptosis, respectively. We found that none of these inhibitors impeded ferroptosis of Gpx4-deficient Treg cells (Figures 3F and S3E). Further, we examined whether transgenic expression of Bcl2 can rescue a survival defect of Gpx4-deficient Treg cells by crossing *Foxp3*$^{Cre}$*Gpx4*$^{fl/fl}$ mice with mice expressing a *Bcl2* transgene in lymphocytes (designated as *Foxp3*$^{Cre}$*Gpx4*$^{fl/fl}$*Bcl2*$^{Tg}$ mice). *Foxp3*$^{Cre}$*Gpx4*$^{fl/fl}$*Bcl2*$^{Tg}$ mice displayed normal frequencies and numbers of Treg cells at steady state (Figure S3F), whereas

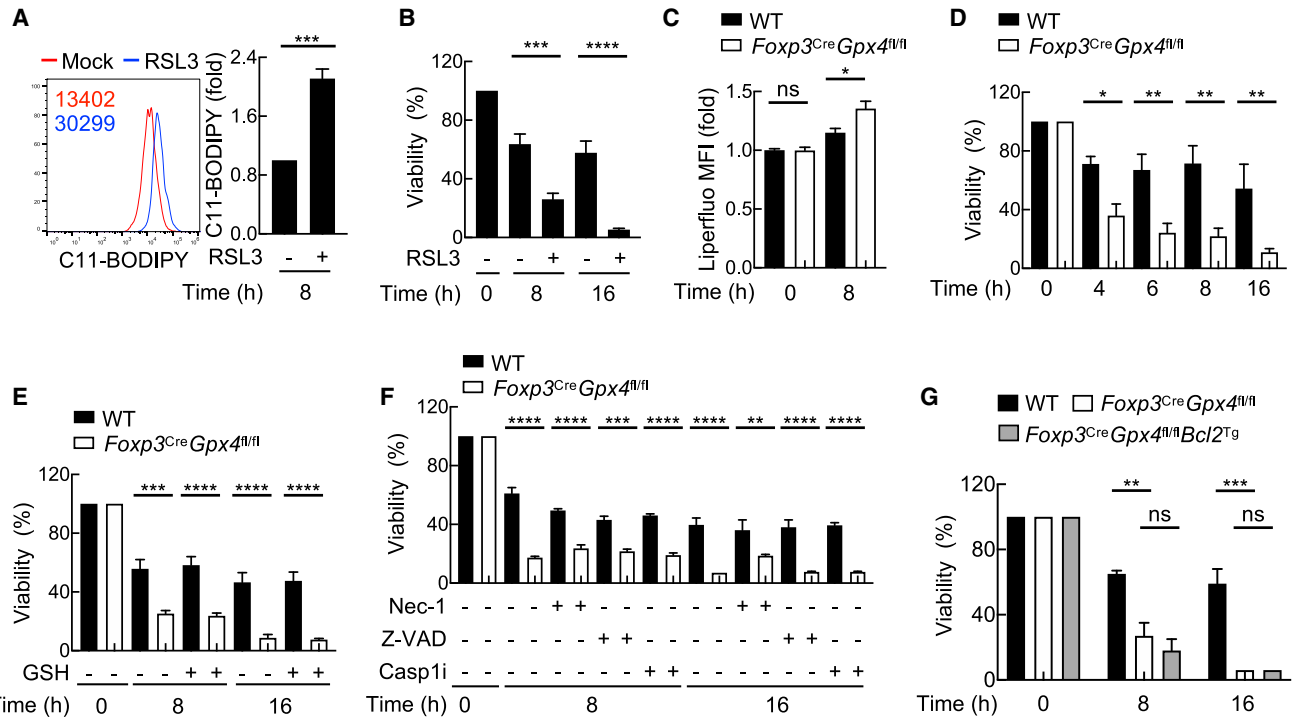


**Figure 3. Gpx4 deficiency evokes lipid peroxidation and ferroptosis of activated Treg cells**

(A) Flow cytometry analysis of C11-BODIPY in WT Treg cells treated with mock or RSL3 (10 μM) in the presence of α-CD3-CD28 and IL-2 for 8 h. Numbers in graphs indicate C11-BODIPY MFI. Right: fold changes of C11-BODIPY MFI on Treg cells (n = 4 each group).

(B) Viability, relative to untreated, of WT Treg cells treated with 10 μM RSL3 in the presence of α-CD3-CD28 and IL-2 for the indicated time points (n = 4 each group).

(C) Fold changes of Liperfluo MFI in WT and *Foxp3*$^{Cre}$*Gpx4*$^{fl/fl}$ Treg cells stimulated with α-CD3-CD28 and IL-2 for the indicated time points (n = 5 each group).

(D) Viability, relative to untreated, of WT and *Foxp3*$^{Cre}$*Gpx4*$^{fl/fl}$ Treg cells stimulated with α-CD3-CD28 and IL-2 for the indicated time points (n = 4 each group).

(E) Relative viability of WT and *Foxp3*$^{Cre}$*Gpx4*$^{fl/fl}$ Treg cells treated with or without 1 mM GSH in the presence of α-CD3-CD28 and IL-2 for the indicated time points (n = 3 each group).

(F) Relative viability of WT and *Foxp3*$^{Cre}$*Gpx4*$^{fl/fl}$ Treg cells treated with or without 10 μM necrostatin-1 (Nec-1), 10 μM Z-VAD-FMK (Z-VAD), or 30 μM caspase-1 inhibitor (Casp1i) in the presence of α-CD3-CD28 and IL-2 for the indicated time points (n = 3 each group).

(G) Relative viability of WT, *Foxp3*$^{Cre}$*Gpx4*$^{fl/fl}$, and *Foxp3*$^{Cre}$*Gpx4*$^{fl/fl}$*Bcl2*$^{Tg}$ Treg cells stimulated with α-CD3-CD28 and IL-2 for the indicated time points.

Data are representative of two (G) or at least three (A–F) independent experiments. Data are mean ± SEM. The p values are determined by two-tailed Student's t test (A) or one-way ANOVA with Tukey's multiple-comparison test (B–G). *p < 0.05, **p < 0.01, ***p < 0.001, ****p < 0.0001. ns, not significant.

transgenic expression of Bcl2 failed to restore ferroptosis of activated Gpx4-deficient Treg cells (Figure 3G). Therefore, Gpx4 deficiency drives ferroptosis of activated Treg cells independent of cellular GSH availability and other cell-death programs.

## Lipid peroxides and iron promote ferroptosis of Gpx4-deficient Treg cells

Multiple factors orchestrate initiation and progression of ferroptotic cell death (Stockwell et al., 2017). To characterize the key components involved in ferroptosis of Gpx4-deficient Treg cells, we examined the effects of pharmaceuticals targeting biosynthesis of polyunsaturated fatty acids (PUFAs), lipid peroxidation, and iron availability. Long-chain-fatty-acid-CoA ligase 4 (ACSL4) is an enzyme that catalyzes biosynthesis of PUFAs to facilitate ferroptosis (Doll et al., 2017; Kagan et al., 2017). We treated WT and Gpx4-deficient Treg cells with pioglitazone (PIO), which suppresses ACSL4 activity (Kim et al., 2001), and found that ferroptotic cell death of Gpx4-deficient Treg cells was not substantially affected by PIO treatment (Figure S4A). This suggests that ACSL4 is dispensable to induce ferroptosis of Gpx4-deficient Treg cells.

To test the effects of neutralizing cellular lipid peroxides on Treg cell ferroptosis, we treated Treg cells with lipid radical scavengers including α-Tocopherol (α-Toc), ferrostatin-1 (Fer-1), and liproxstatin-1 (Lip-1) (Stockwell et al., 2017). Notably, α-Toc treatment rectified aberrant lipid peroxidation in activated Gpx4-deficient Treg cells (Figure 4A) and prevented their ferroptosis (Figure 4B). Similarly, both Fer-1 and Lip-1 rescued ferroptosis of activated Gpx4-deficient Treg cells (Figures 4C and S4B). Having established the rescue effect of Fer-1 on Gpx4-deficiency-induced Treg ferroptosis, we next sought to assess whether Fer-1 restores the suppressive function of Gpx4-deficient Treg cells *in vitro*. We cocultured dendritic cells (DCs) and naive CD4$^+$ T cells with WT or Gpx4-deficient Treg cells in the presence or absence of Fer-1 and α-CD3. WT Treg cells suppressed the generation of CellTrace$^{low}$CD4$^+$ T cells (Figure 4D), indicative of reduced cell expansion, but Gpx4-deficient Treg cells failed to do so (Figure 4D). Of note, Fer-1 treatment did

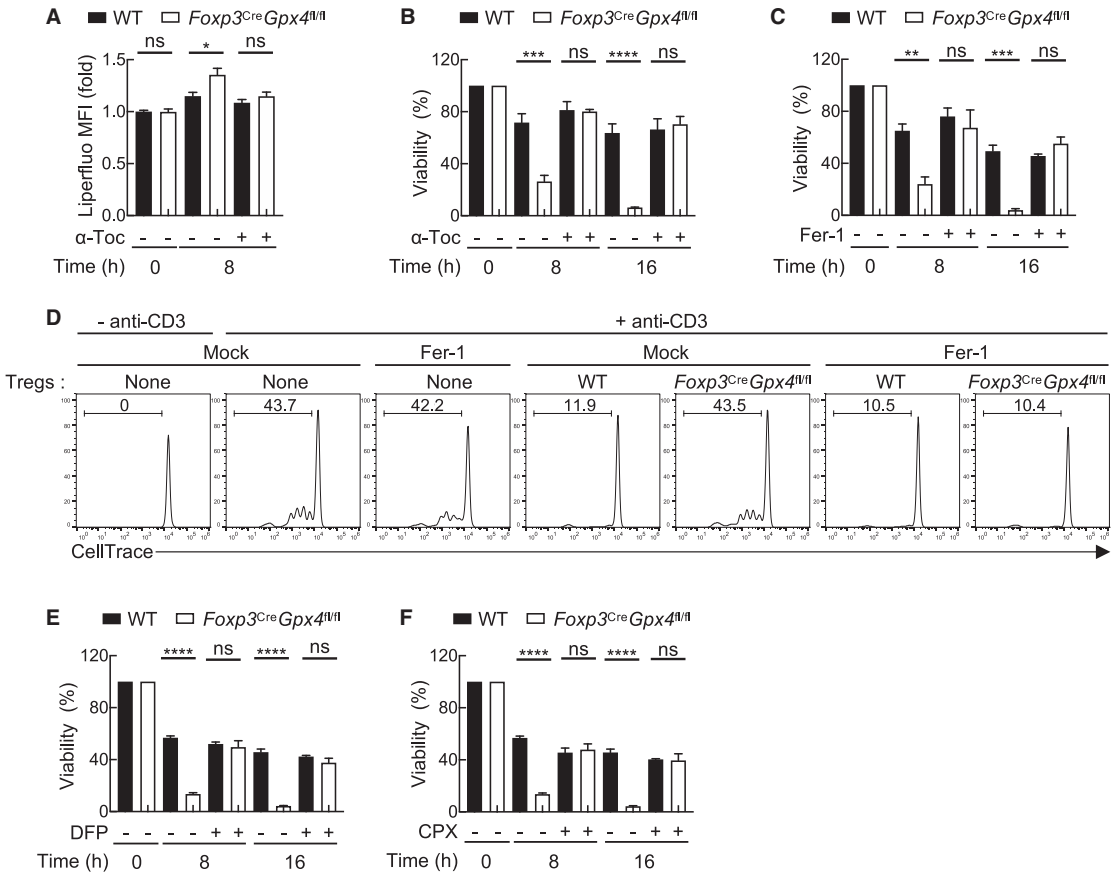


**Figure 4. Lipid peroxides and iron promote ferroptosis of Gpx4-deficient Treg cells**

(A) Fold changes of Liperfluo MFI in WT and *Foxp3*$^{Cre}$*Gpx4*$^{fl/fl}$ Treg cells treated with or without 10 μM α-Toc in the presence of α-CD3-CD28 and IL-2 for the indicated time points (n = 5 each group).

(B) Relative viability of WT and *Foxp3*$^{Cre}$*Gpx4*$^{fl/fl}$ Treg cells treated with or without 10 μM α-Toc in the presence of α-CD3-CD28 and IL-2 for the indicated time points (n = 3 each group).

(C) Relative viability of WT and *Foxp3*$^{Cre}$*Gpx4*$^{fl/fl}$ Treg cells treated with or without ferrostatin-1 (Fer-1; 10 μM) in the presence of α-CD3-CD28 and IL-2 for the indicated time points (n = 3 each group).

(D) Flow cytometry analysis of CellTrace-labeled naive CD4$^+$ T cells cocultured without or with *Foxp3*$^{Cre}$ or *Foxp3*$^{Cre}$*Gpx4*$^{fl/fl}$ Treg cells in the presence or absence of α-CD3 and/or Fer-1 for 3 days. Numbers in gates indicate the percentage of CellTrace-diluted cells.

(E and F) Relative viability of WT and *Foxp3*$^{Cre}$*Gpx4*$^{fl/fl}$ Treg cells treated without or with 70 μM deferiprone (DFP) (E) or 1 μM ciclopirox (CPX) (F) in the presence of α-CD3-CD28 and IL-2 for the indicated time points (n = 3 each group).

Data are representative of at least three independent experiments. Data are mean ± SEM. The p values are determined by one-way ANOVA with Tukey's multiple-comparison test (A–C, E, and F). *p < 0.05, **p < 0.01, ***p < 0.001, ****p < 0.0001. ns, not significant.

not affect expansion of CD4$^+$ T cells in the absence of Treg cells, whereas it restored the capability of Gpx4-deficient Treg cells in repressing CD4$^+$ T cell expansion (Figure 4D). Thus, Gpx4 restrains accumulation of lipid peroxides in activated Treg cells and prevents their ferroptosis.

Transferrin receptor protein 1 (TfR1; also known as CD71) imports iron to fuel the Fenton reaction in promoting hydroxyl radical generation and ferroptosis (Feng et al., 2020). Gpx4-deficient Treg cells showed enhanced expression of CD71 (Figure S4C), suggestive of increased iron uptake. To determine the effects of blocking iron availability on Treg cell ferroptosis, we treated WT and Gpx4-deficient Treg cells with the potent iron chelators deferiprone (DFP) (Devos et al., 2014) and ciclopirox (CPX) (Dixon et al., 2012). Notably, DFP treatment suppressed ferroptosis of activated Gpx4-deficient Treg cells (Figure 4E). A similar rescue effect was also observed in CPX-treated Gpx4-deficient Treg cells (Figure 4F). This indicates that iron plays a crucial role in triggering ferroptosis of Treg cells lacking Gpx4.

## Gpx4-deficient Treg cells elevate mitochondrial superoxide generation

We next sought to determine the molecular mechanisms underlying Gpx4-dependent regulation of lipid peroxidation and ferroptosis in Treg cells. To this aim, we performed RNA sequencing (RNA-seq) to profile the transcriptome of resting WT, Gpx4-deficient Treg cells, and those stimulated with α-CD3-CD28 antibodies for 4 h. Resting Gpx4-deficient Treg

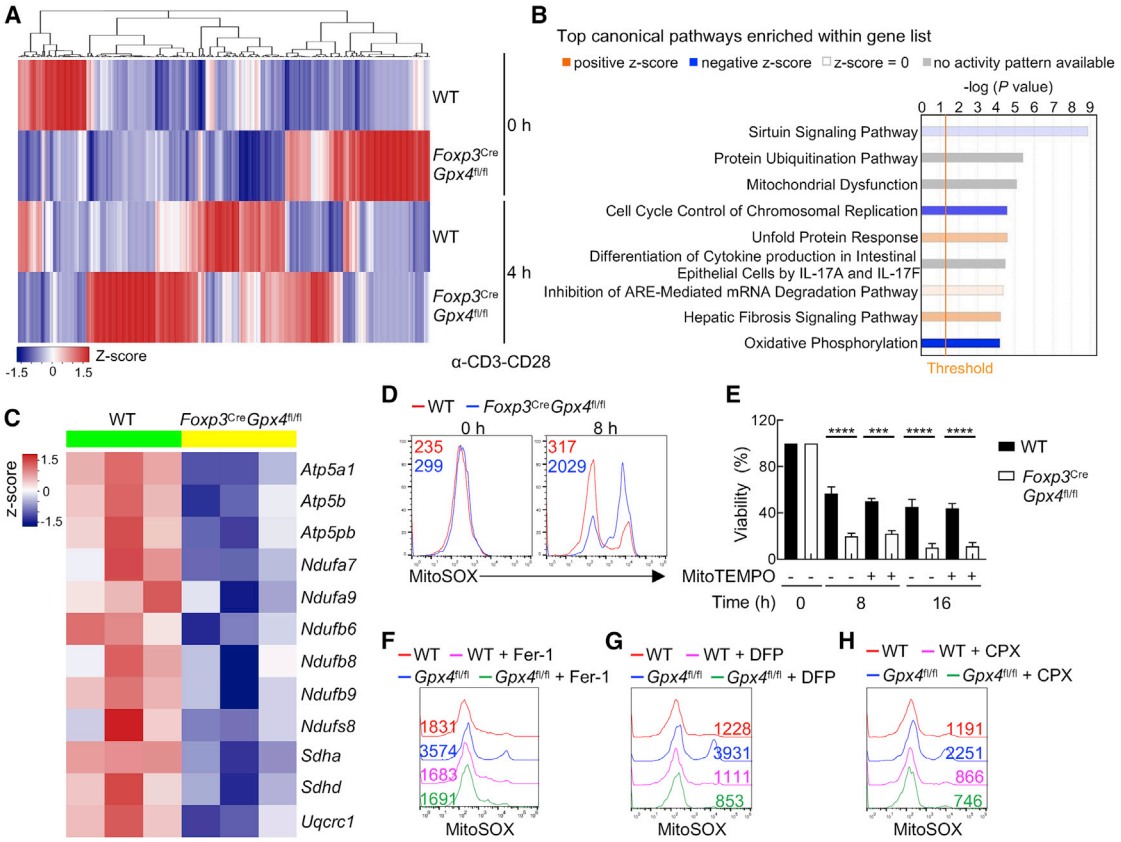


**Figure 5. Gpx4-deficient Treg cells elevate generation of mitochondrial ROS**

(A) Heatmap showing the DEGs in WT and Gpx4-deficient Treg cells with or without α-CD3-CD28 stimulation for 4 h.

(B) IPA results indicating the top canonical pathways enriched in the DEGs in resting Gpx4-deficient Treg cells.

(C) Heatmap showing the DEGs enriched in oxidative phosphorylation in resting Gpx4-deficient Treg cells.

(D) Flow cytometry analysis of MitoSOX, a probe of mitochondrial ROS, in resting WT and *Foxp3*$^{Cre}$*Gpx4*$^{fl/fl}$ Treg cells and those stimulated with α-CD3-CD28 and IL-2 for 8 h. Numbers in graphs indicate MitoSOX MFI.

(E) Relative viability of WT and *Foxp3*$^{Cre}$*Gpx4*$^{fl/fl}$ Treg cells stimulated with or without MitoTEMPO in the presence of α-CD3-CD28 and IL-2 for the indicated time points.

(F) Flow cytometry analysis of MitoSOX in WT and *Foxp3*$^{Cre}$*Gpx4*$^{fl/fl}$ Treg cells stimulated with or without 10 μM Fer-1 in the presence of α-CD3-CD28 and IL-2 for 8 h.

(G and H) Flow cytometry analysis of MitoSOX in WT and *Foxp3*$^{Cre}$*Gpx4*$^{fl/fl}$ Treg cells stimulated with or without 70 μM DFP (G) or 1 μM CPX (H) in the presence of α-CD3-CD28 and IL-2 for 8 h.

Data are representative of one (A–C) or at least three (D–H) independent experiments. Data are mean ± SEM. The p values are determined by one-way ANOVA with Tukey's multiple-comparison test (E). ***p < 0.001, ****p < 0.0001.

cells showed 182 differentially expressed genes (DEGs; absolute $\log_2$ fold change [FC] > 1.2 and false discovery rate [FDR] < 0.05), whereas those stimulated with α-CD3-CD28 antibodies had 1,082 DEGs relative to WT counterparts (Figures 5A and S5A). Among the top 20 most significant genes changed in resting Gpx4-deficient Treg cells (Figure S5A), we noted increased expression of several key stress-response genes including *Hspa1* and *Dnajb1*. In line with this notion, Ingenuity Pathway Analysis (IPA) revealed that unfolded protein response and hepatic fibrosis signaling pathways were significantly enriched as upregulated canonical pathways in resting Gpx4-deficient Treg cells (Figure 5B). Downregulated canonical pathways enriched in Gpx4-deficient Treg cells included the sirtuin signaling pathway, cell-cycle control of chromosomal replication, and oxidative phosphorylation (Figure 5B). Of note, Gpx4-deficient Treg cells showed downregulated expression of key genes implicated in the mitochondrial electron transport chain (ETC) and tricarboxylic acid cycle (TCA) in the program of oxidative phosphorylation (Figure 5C). These results suggest that Gpx4 plays a role in the regulation of Treg mitochondrial homeostasis.

To assess the impact of Gpx4 deficiency on mitochondrial fitness, we measured mitochondrial mass, membrane potential, and superoxide production with MitoTracker, tetramethylrhodamine methyl ester (TMRM), and MitoSOX, respectively. We found that WT and Gpx4-deficient Treg cells had comparable levels of mitochondrial mass and membrane potential (Figures S5B and S5C) and generation of mitochondrial superoxide (Figure 5D) at steady state. Strikingly, Gpx4-deficient Treg cells markedly elevated generation of mitochondrial superoxide upon TCR/CD28 co-stimulation (Figure 5D) but retained normal

levels of MitoTracker and TMRM (Figures S5B and S5C). To assess the contribution of mitochondrial superoxide to Treg cell ferroptosis, WT and Gpx4-deficient Treg cells were pre-treated with MitoTEMPO, a well-documented mitochondria-specific superoxide scavenger, followed by TCR/CD28 co-stimulation. Unexpectedly, MitoTEMPO treatment failed to rescue ferroptosis of Gpx4-deficient Treg cells (Figure 5E). We next examined the extent to which lipid peroxides and free iron contribute to aberrant production of mitochondrial superoxide in Gpx4-deficient Treg cells. Notably, neutralization of lipid peroxides by Fer-1 (Figure 5F) and blockade of iron availability by the iron chelators DFP and CPX (Figures 5G and 5H) rectified the generation of excessive mitochondrial superoxide in activated Gpx4-deficient Treg cells. Collectively, Treg cells need Gpx4 to neutralize lipid peroxides in maintaining mitochondrial fitness.

## IL-1β derived from Gpx4-deficient Treg cells facilitates $T_H17$ responses

Ferroptotic cells may contribute to pathological development of multiple diseases via releasing proinflammatory cytokines (Proneth and Conrad, 2019). We noted that activated Gpx4-deficient Treg cells showed increased expression of various chemokines and proinflammatory cytokines (Figure 6A), including *Ccl19*, *Ccl6*, *Il1b*, *Cxcl2*, *Ccl5*, and *Csf1*, concomitant with reduction of *Tnfsf10*, *Il31*, *Cxcl13*, and *Il33* (Figure 6A). Interestingly, IPA revealed that the canonical pathway of lipopolysaccharide (LPS)/IL-1-mediated inhibition of RXR function was significantly enriched as an upregulated canonical pathway in activated Gpx4-deficient Treg cells (Figure 6B). Given the importance of IL-1β in regulating a variety of immune cells (Van Den Eeckhout et al., 2021), we further validated expression of IL-1β in Gpx4-deficient Treg cells. Resting WT and Gpx4-deficient Treg cells had comparable expression of *Il1b* (Figure 6C), whereas α-CD3-CD28 stimulation significantly increased expression of *Il1b* in Gpx4-deficient Treg cells as early as 4 h (Figure 6C). Consistent with this finding, concentration of IL-1β in the conditioned medium from activated Gpx4-deficient Treg cells was higher than that from WT counterparts (Figure 6D).

IL-1β drives the generation of pathogenic $T_H17$ cells in the presence of IL-6 and IL-23 (Chung et al., 2009). To determine the effects of Treg-derived IL-1β on $T_H17$ responses, we harvested the supernatant from α-CD3-CD28-stimulated WT and Gpx4-deficient Treg cells to culture WT DCs and naive $CD4^+$ T cells in the presence of IL-6 and IL-23 for an additional 5 days. We found that the conditioned medium from activated Gpx4-deficient Treg cells, but not from activated WT counterparts, promoted the generation of IL-17-producing $CD4^+$ T cells (Figures 6E and S6A), without affecting IFN-γ production (Figures 6E and S6A). Moreover, addition of IL-1β-neutralizing antibody notably suppressed the generation of IL-17-producing $CD4^+$ T cells induced by the conditioned medium from activated Gpx4-deficient Treg cells (Figure 6E). To examine whether neutralization of lipid peroxides affects IL-1β production, we treated WT and *Foxp3*$^{Cre}$*Gpx4*$^{fl/fl}$ Treg cells with α-Toc or Fer-1 upon α-CD3-CD28 stimulation. Both α-Toc and Fer-1 diminished expression of *Il1b* in activated Gpx4-deficient Treg cells (Figure 6F). Importantly, the conditioned medium from Fer-1-treated Gpx4-deficient Treg cells failed to induce IL-17 production by $CD4^+$ T cells (Figure 6G), compared to that from activated Gpx4-deficient Treg cells. Thus, ferroptotic Gpx4-deficient Treg cells elevate IL-1β production with a potential promotion of $T_H17$ responses.

Cellular ROS can induce or be induced by activation of ERK signaling in different biological processes. We next examined whether the ERK signaling pathway induces lipid peroxidation and IL-1β production in Gpx4-deficient Treg cells. WT and Gpx4-deficient Treg cells showed comparable phosphorylation of ERK in response to α-CD3-CD28 stimulation (Figure S6B), indicating that Gpx4 is dispensable for ERK activation. We next used the MEK/ERK inhibitor U0126 to treat WT and Gpx4-deficient Treg cells and examined its impact on lipid peroxidation and IL-1β production. As expected, U0126 effectively inhibited ERK phosphorylation (Figure S6C). Importantly, it repressed the generation of lipid peroxides (Figure S6D) and expression of *Il1b* (Figure S6E) in Gpx4-deficient Treg cells, whereas rescuing their survival defect (Figure S6F). However, a recent study indicates that U0126 suppresses ferroptosis via promoting an ERK-independent antioxidant property (Gao et al., 2015). To test this possibility, we examined the effect of LY3214996, a potent and selective ATP-competitive ERK inhibitor (Bhagwat et al., 2020), on Treg ferroptosis. Notably, LY3214996 did not rescue ferroptosis of Gpx4-deficient Treg cells (Figure S6G). To further confirm the independence of ERK in inducing Treg ferroptosis, we used small interfering RNA (siRNA) targeting ERK1/2 (siERK) to knock down their expression in WT Treg cells, followed by RSL3 treatment. Despite ERK siRNA resulting in marked reduction of ERK1/2, it failed to prevent RSL3-induced Treg ferroptosis (Figure S6H). Collectively, accumulated lipid peroxides, but not ERK activation, induce ferroptosis and IL-1β production in activated Gpx4-deficient Treg cells.

## Gpx4 sustains Treg cell suppression of antitumor immune responses

Treg cells are crucial to promote tumor immune evasion (Togashi et al., 2019). Inducing apoptosis of intratumoral Treg cells unexpectedly enhances their immunosuppressive function and consequently promotes tumor growth (Maj et al., 2017). To test the potential involvement of Gpx4 and lipid peroxidation in intratumoral Treg cells, we first examined Gpx4 expression and generation of lipid peroxides in intratumoral Treg cells from WT mice bearing B16 melanoma. The proportions of Treg cells in the melanomas were markedly enhanced compared to those in spleens (Figure S7A). Of note, intratumoral Treg cells showed increased levels of lipid peroxides (Figure S7B) and expression of Gpx4 (Figure S7C) relative to splenic counterparts, suggesting that Gpx4 may regulate the generation of lipid peroxides in intratumoral Treg cells. To determine the effects of Gpx4-deficient Treg cells on antitumor immunity, we inoculated WT and *Foxp3*$^{Cre}$*Gpx4*$^{fl/fl}$ mice with B16.F10 melanoma or MC38 colon adenocarcinoma cells and then monitored tumor growth. *Foxp3*$^{Cre}$*Gpx4*$^{fl/fl}$ mice showed compromised B16 melanoma growth (Figure 7A), associated with the reduced tumor weight (Figure 7B), relative to those in WT counterparts. Similarly, growth of MC38 tumors (Figure 7C) and tumor weight (Figure 7D) was notably repressed in *Foxp3*$^{Cre}$*Gpx4*$^{fl/fl}$ mice. In line with the diminished tumor burden,

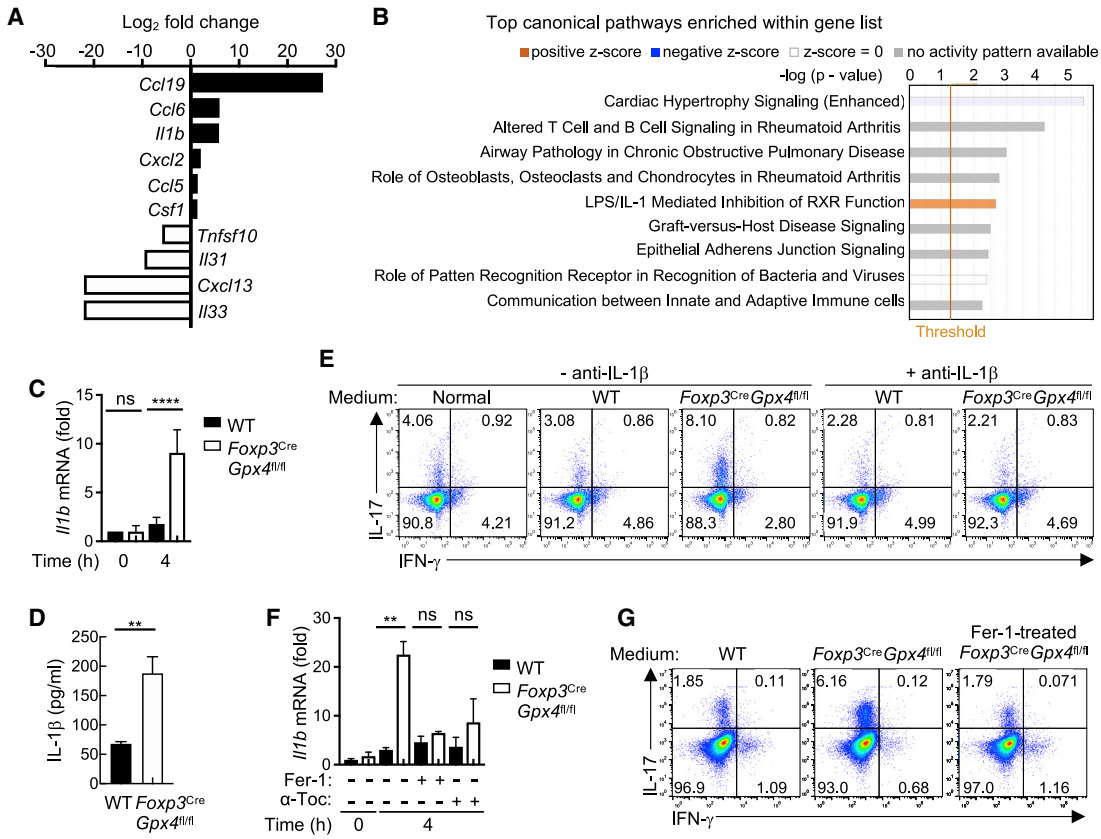


**Figure 6. Loss of Gpx4 enables Treg cells to enhance IL-1β production**

(A) Fold changes of cytokines and chemokines differentially expressed in Gpx4-deficient Treg cells stimulated with α-CD3-CD28 for 4 h compared to WT counterparts (n = 3 each group).

(B) IPA results indicating the top canonical pathways enriched in the DEGs in activated Gpx4-deficient Treg cells.

(C) Relative expression of *Il1b* mRNA in WT and *Foxp3*$^{Cre}$*Gpx4*$^{fl/fl}$ Treg cells stimulated with α-CD3-CD28 for 0 h or 4 h (n = 3 each group).

(D) IL-1β concentration in the conditioned medium from WT and Treg cells stimulated with α-CD3-CD28 for 18 h.

(E) Expression of IL-17 and IFN-γ in CD4$^+$ T cells cocultured with DCs in the normal medium or the conditioned medium from activated WT or *Foxp3*$^{Cre}$*Gpx4*$^{fl/fl}$ Treg cells under stimulation of α-CD3, α-CD28, α-IL-2, IL-6, and IL-23 in the presence or absence of IL-1β-neutralizing antibody for 5 days.

(F) Relative expression of *Il1b* mRNA in WT and *Foxp3*$^{Cre}$*Gpx4*$^{fl/fl}$ Treg cells treated with or without Fer-1 (10 μM) or α-Toc (10 μM) upon α-CD3-CD28 stimulation.

(G) Expression of IL-17 and IFN-γ in CD4$^+$ T cells cocultured with the conditioned medium from activated WT, activated *Foxp3*$^{Cre}$*Gpx4*$^{fl/fl}$ Treg cells, or activated *Foxp3*$^{Cre}$*Gpx4*$^{fl/fl}$ Treg cells treated with 10 μM Fer-1 in the presence of α-CD3, α-CD28, α-IL-2, IL-6, and IL-23 for 5 days.

Data are representative of one (A and B), two (E and G), or at least three (C, D, and F) independent experiments. Data are mean ± SEM. The p values are determined by two-tailed Student's t test (D) or one-way ANOVA with Tukey's multiple-comparison test (C and F). **p < 0.01, ****p < 0.0001. ns, not significant. Numbers in quadrants indicate the percentage of cells.

mice with Treg-specific deletion of Gpx4 showed increased proportions of tumor-infiltrating T cells (Figure S7D), characterized by higher ratios of cytotoxic CD8$^+$ T cells to CD4$^+$ T cells (Figures 7E, 7F, and S7E). These data indicate that Treg-specific deletion of Gpx4 potentiates the antitumor immune response.

On the basis of the reduced tumor growth in *Foxp3*$^{Cre}$*Gpx4*$^{fl/fl}$ mice, we hypothesized that Gpx4 deficiency compromises the immunosuppressive function of intratumoral Treg cells. In support of this idea, tumor-infiltrating CD8$^+$ T cells from *Foxp3*$^{Cre}$*Gpx4*$^{fl/fl}$ mice showed increased production of the antitumor effectors IFN-γ (Figure 7G) and tumor necrosis factor α (TNF-α) (Figure 7H), relative to WT counterparts. Similarly, the tumors from *Foxp3*$^{Cre}$*Gpx4*$^{fl/fl}$ mice had elevated proportions of intratumoral CD4$^+$ T cells producing TNF-α or IFN-γ (Figures S7F and S7G). This suggested that Treg cells need to upregulate Gpx4 expression to sustain their functionality and survival in the TME. In support of this idea, intratumoral Gpx4-deficient Treg cells had slightly diminished expression of Foxp3 (Figure 7I), whereas retaining intact expression of the Treg marker PD-1 (Figure S7H) relative to WT counterparts. Moreover, *Foxp3*$^{Cre}$*Gpx4*$^{fl/fl}$ mice displayed reduced proportions of intratumoral Treg cells (Figure 7J), associated with increased cell death (Figure S7I), leading to increased ratios of intratumoral CD8$^+$ T cells to Treg cells (Figure 7J). In contrast, the spleens from tumor-bearing WT and *Foxp3*$^{Cre}$*Gpx4*$^{fl/fl}$ mice had comparable ratios of CD8$^+$ T cells to Treg cells (Figure S7J). To determine whether Gpx4-deficiency-induced Treg ferroptosis is responsible for the enhanced tumor regression, we administered Lip-1 to *Foxp3*$^{Cre}$*Gpx4*$^{fl/fl}$ mice bearing MC38 tumor cells every day and assessed its impact

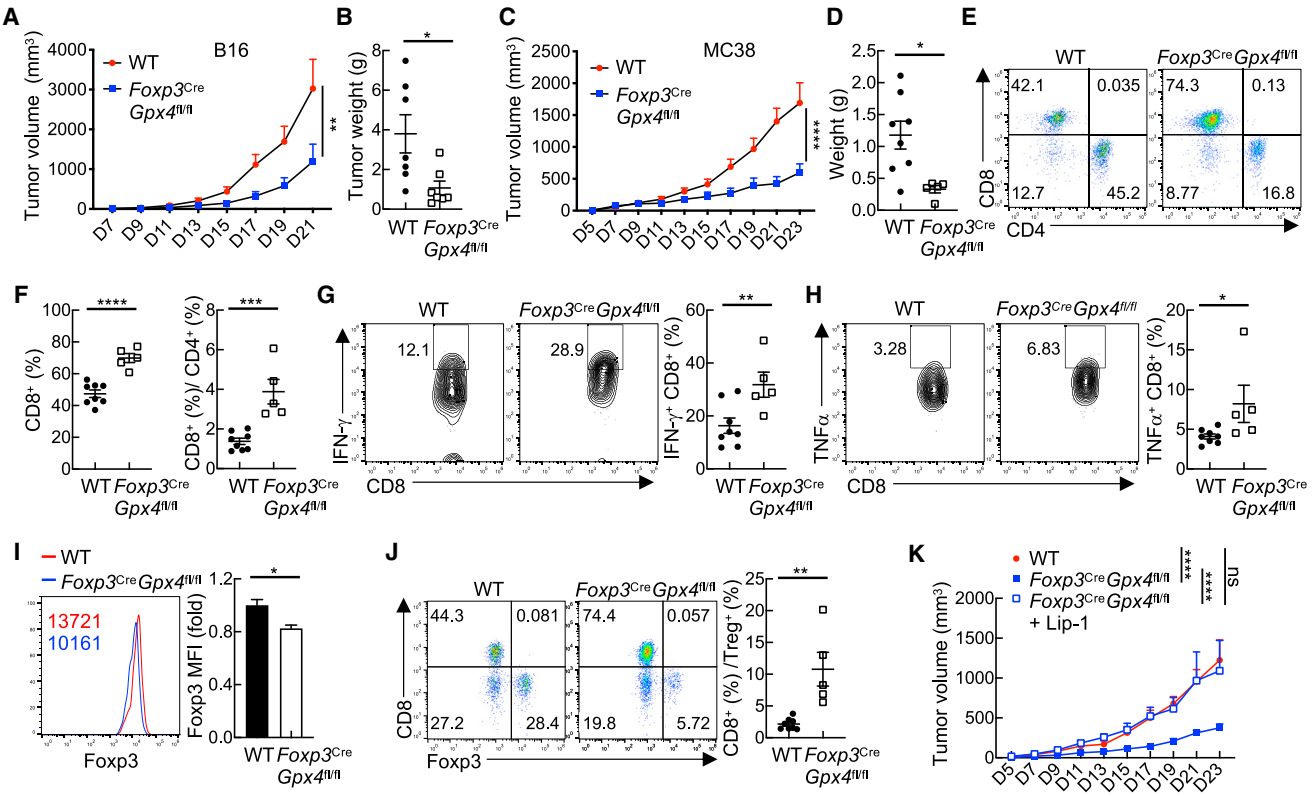


**Figure 7. Treg-specific deletion of Gpx4 potentiates antitumor immune responses**

(A) Tumor volume of WT and *Foxp3*$^{Cre}$*Gpx4*$^{fl/fl}$ mice subcutaneously inoculated with B16.F10 melanoma cells (n = 7 each group).

(B) Weight of the tumors collected from WT and *Foxp3*$^{Cre}$*Gpx4*$^{fl/fl}$ mice in (A).

(C) Tumor volume of WT (n = 8) and *Foxp3*$^{Cre}$*Gpx4*$^{fl/fl}$ (n = 5) mice subcutaneously inoculated with MC38 tumor cells.

(D) Weight of the tumors collected from WT (n = 8) and *Foxp3*$^{Cre}$*Gpx4*$^{fl/fl}$ (n = 5) mice in (C).

(E and F) Flow cytometry analysis of intratumoral CD4$^+$ and CD8$^+$ T cells from WT and *Foxp3*$^{Cre}$*Gpx4*$^{fl/fl}$ mice subcutaneously inoculated with MC38 tumor cells (E). Proportions of intratumoral CD8$^+$ T cells (left) and ratios of CD8$^+$ (%) to CD4$^+$ (%) (right) from WT (n = 8) and *Foxp3*$^{Cre}$*Gpx4*$^{fl/fl}$ (n = 5) mice (F).

(G) Flow cytometry analysis of IFN-γ-producing CD8$^+$ T cells in MC38 tumors from WT and *Foxp3*$^{Cre}$*Gpx4*$^{fl/fl}$ mice. Right: proportions of IFN-γ-producing CD8$^+$ T cells from WT (n = 8) and *Foxp3*$^{Cre}$*Gpx4*$^{fl/fl}$ (n = 5) mice.

(H) Flow cytometry analysis of TNF-α in intratumoral CD8$^+$ T cells from WT and *Foxp3*$^{Cre}$*Gpx4*$^{fl/fl}$ mice bearing MC38 tumors. Right: proportions of TNF-α-producing CD8$^+$ T cells in tumors from WT (n = 8) and *Foxp3*$^{Cre}$*Gpx4*$^{fl/fl}$ (n = 5) mice.

(I) Expression of Foxp3 in intratumoral Treg cells from tumor-bearing WT and *Foxp3*$^{Cre}$*Gpx4*$^{fl/fl}$ mice. Numbers in graphs indicate Foxp3 MFI. Right: fold changes of Foxp3 MFI in intratumoral Treg cells from WT (n = 8) and *Foxp3*$^{Cre}$*Gpx4*$^{fl/fl}$ (n = 5) mice.

(J) Flow cytometry analysis of intratumoral CD8$^+$ T cells and Treg cells from WT and *Foxp3*$^{Cre}$*Gpx4*$^{fl/fl}$ mice subcutaneously inoculated with MC38 tumor cells. Right: ratios of intratumoral CD8$^+$ T cells (%) to Treg cells (%) from WT (n = 8) and *Foxp3*$^{Cre}$*Gpx4*$^{fl/fl}$ (n = 5) mice.

(K) Tumor volume of WT (n = 4), *Foxp3*$^{Cre}$*Gpx4*$^{fl/fl}$ (n = 4), and Lip-1-treated *Foxp3*$^{Cre}$*Gpx4*$^{fl/fl}$ (n = 3) mice subcutaneously inoculated with MC38 tumor cells.

Data are representative of two independent experiments. Data are mean ± SEM. The p values are determined by two-way ANOVA with Bonferroni's multiple-comparison test (A, C, and K) or two-tailed Student's t test (B, D, and F–J). *p < 0.05, **p < 0.01, ***p < 0.001, ****p < 0.0001. ns, not significant. Numbers in quadrants or gates indicate the percentage of cells.

on tumor growth. Notably, Lip-1-administered *Foxp3*$^{Cre}$*Gpx4*$^{fl/fl}$ mice had significantly augmented tumor growth (Figure 7K), accompanied by elevated tumor weight and decreased ratios of CD8$^+$ T cells to Treg cells in density (Figure S7K), compared to those without Lip treatment. This indicates that Gpx4 sustains survival and immunosuppressive function of intratumoral Treg cells to facilitate tumor immune evasion.

## DISCUSSION

Coordination of microenvironmental cues and cell-intrinsic signaling and metabolic networks is crucial for Treg cells in sustaining their suppressive function under different immunological settings. Continued oxidative stress represents a key microenvironmental factor that not only induces genetic and behavioral changes in cancer cells but also differentially shapes the function of various immune cells (Lyssiotis and Kimmelman, 2017). In comparison to effector T cells, Treg cells exhibit reduced susceptibility to oxidative stress (Mougiakakos et al., 2009, 2011), contributing to elevated frequencies and function of Treg cells in the high oxidative stress TME (Facciabene et al., 2012). Moreover, activated and intratumoral Treg cells enhance lipid biosynthesis (Pacella et al., 2018) and fatty acid oxidation (Field et al., 2020; Wang et al., 2020), which potentially elevates intracellular

ROS production and induces oxidative stress. However, the mechanisms governing Treg cell redox homeostasis in response to changes in intra- and extracellular conditions remain elusive. We have now established a novel role for Gpx4 in Treg cells, which keeps lipid peroxidation in check to prevent ferroptosis and sustain Treg cell function in regulating immune tolerance and antitumor immunity (Figure S7L).

Signal-induced production of cellular ROS in T cells affects multiple aspects of T cell immunity including T cell activation (Sena et al., 2013), differentiation (Gerriets et al., 2015; Yang et al., 2018), and function (Beier et al., 2015). It is well established that mitochondria function as a key source of cellular ROS and energy crucial for maintaining Treg cell homeostasis and suppressive function (Beier et al., 2015; Weinberg et al., 2019; Yu et al., 2018). However, little is known about the regulation and function of lipid ROS in T cells. In a recent study, it was shown that deletion of Gpx4 in total $CD4^+$ and $CD8^+$ T cells causes accumulation of membrane lipid peroxides and induces ferroptosis of conventional T cells (Matsushita et al., 2015) but not survival and homeostatic proliferation of Treg cells (Matsushita et al., 2015). It remains elusive whether Gpx4 regulates cellular redox homeostasis of antigen-stimulated Treg cells in the control of immune tolerance and antitumor immune responses. By generating mice with Treg-specific deletion of Gpx4, we found that loss of Gpx4 in Treg cells impaired suppression of $T_H1$ and $T_H17$ responses in a tissue-context-dependent manner, without substantially affecting their survival at steady state. In contrast, TCR/CD28 co-stimulation triggered excessive accumulation of lipid peroxides and subsequent ferroptosis in Treg cells lacking Gpx4, which was restored by lipid radical scavengers and iron chelators. Our data further uncovered that ferroptotic Treg cells aberrantly produced proinflammatory factors such as IL-1β, and in turn promoted $T_H17$ responses. Thus, Gpx4 is indispensable to protect activated Treg cells from accumulation of lipid peroxides and ferroptosis and sustains Treg cell activation and functionality.

Development of Treg-cell-targeted therapies has been proposed as a promising strategy to enhance antitumor immune responses (Togashi et al., 2019). In the TME, Treg cells enhance immunosuppressive functions by adopting various mechanisms that resist extracellular challenges, including high oxidative stress, limited nutrient availability, low pH, and hypoxia (Speiser et al., 2016). Recent studies highlight that modulating the responsiveness of intratumoral Treg cells to microenvironmental cues disrupts their stability and survival differentially, thereby shaping the outcome of antitumor immunity. For instance, Treg-cell-specific deletion of the receptor neuropilin-1 (Nrp1) impairs the functional stability of Treg cells (Delgoffe et al., 2013) and induces the fragility of intratumoral Treg cells (Overacre-Delgoffe et al., 2017), promoting antitumor immunity and tumor regression. In contrast, induction of Treg cell apoptosis by increasing sensitivity to oxidative stress potentiates the immunosuppressive function of Treg cells and facilitates tumor growth (Maj et al., 2017). However, whether the non-apoptotic form of cell death can impair Treg cell function remains unknown. Here we note that human and mouse Treg cells have elevated expression of the glutathione peroxidase Gpx4 in the TME. Loss of Gpx4 induces Treg cell ferroptosis, a non-apoptotic form of cell death, in response to TCR and co-stimulation. Importantly, mice with Treg-specific deletion of Gpx4 dampen tumor growth with a concomitant enhancement of antitumor immune responses, without causing overt autoimmunity. It has been recently reported that IFN-γ derived from $CD8^+$ T cells induces cancer cell ferroptosis (Wang et al., 2019). Given the implication of IL-1β in regulating the differentiation of $T_H1$, $T_H17$, and $CD8^+$ T cells (Ben-Sasson et al., 2013; Van Den Eeckhout et al., 2021), IL-1β derived from ferroptotic Gpx4-deficient Treg cells may promote the activation of DCs and function of $CD8^+$ T cells in repressing tumor growth (Björkdahl et al., 2000; Fotaki et al., 2017; Zhivaki et al., 2020). Our studies provide evidence indicating that inducing ferroptosis of intratumoral Treg cells by Gpx4 deficiency potentiates antitumor immunity and augments tumor regression.

In summary, we have established a novel cell-intrinsic mechanism by which Gpx4 maintains cellular redox homeostasis in Treg cells. We demonstrated that Gpx4-dependent neutralization of lipid peroxides protects Treg cells from ferroptotic cell death, and in turn sustains Treg cell activation and function in controlling antitumor immunity. Gpx4 deficiency enables ferroptotic Treg cells to enhance production of proinflammatory cytokines, such as IL-1β, which facilitate inflammatory responses. Our studies suggest that inducing of Treg cell lipid peroxidation and ferroptosis may promote the development of a therapeutic strategy to improve cancer treatment.

## STAR★METHODS

Detailed methods are provided in the online version of this paper and include the following:

- KEY RESOURCES TABLE
- RESOURCE AVAILABILITY
  - Lead contact
  - Materials availability
  - Data and code availability
- EXPERIMENTAL MODEL AND SUBJECT DETAILS
  - Mouse strains
  - Subcutaneous implantation of murine MC38 or B16.F10 tumor cells
- METHOD DETAILS
  - Flow cytometry
  - Cell purification and cultures
  - Cell death assay
  - Immunoblot and quantitative RT-PCR
  - Coculture of naive $CD4^+$ T cells and DCs with the medium from activated Treg cells
  - siRNA transfection
  - Treg-mediated suppression of naive $CD4^+$ T cell proliferation
- QUANTIFICATION AND STATISTICAL ANALYSIS
  - RNA sequencing and library preparation
  - RNA-sequencing data processing and analysis
  - Statistical analysis

## SUPPLEMENTAL INFORMATION

Supplemental information can be found online at https://doi.org/10.1016/j.celrep.2021.109235.

## ACKNOWLEDGMENTS

The authors acknowledge J. Trittipo for animal colony managemen, and the Simon Comprehensive Cancer Center FACS core facility for cell sorting and multiplex core facility for cytokine quantification. This work was partially supported by a Showalter Trust Young Investigator Award (to K.Y.). Core facility usage was also supported by IU Simon Comprehensive Cancer Center support grants P30 CA082709 and U54 DK106846. Support provided by the Herman B Wells Center was in part from the Riley Children's Foundation.

## AUTHOR CONTRIBUTIONS

C.X. designed and performed cellular, molecular, and biochemical experiments and contributed to the writing of the manuscript; S.S. performed molecular experiments; T.J. and J.Z. performed bioinformatic analysis; R.Q. and S.Z. contributed critical insight to this study; and K.Y. designed experiments, wrote the manuscript, and supervised the work.

## DECLARATION OF INTERESTS

The authors declare no competing interests.

Received: November 9, 2020
Revised: April 14, 2021
Accepted: May 19, 2021
Published: June 15, 2021

## REFERENCES

Beier, U.H., Angelin, A., Akimova, T., Wang, L., Liu, Y., Xiao, H., Koike, M.A., Hancock, S.A., Bhatti, T.R., Han, R., et al. (2015). Essential role of mitochondrial energy metabolism in Foxp3$^+$ T-regulatory cell function and allograft survival. FASEB J. *29*, 2315–2326.

Ben-Sasson, S.Z., Hogg, A., Hu-Li, J., Wingfield, P., Chen, X., Crank, M., Caucheteux, S., Ratner-Hurevich, M., Berzofsky, J.A., Nir-Paz, R., and Paul, W.E. (2013). IL-1 enhances expansion, effector function, tissue localization, and memory response of antigen-specific CD8 T cells. J. Exp. Med. *210*, 491–502.

Bhagwat, S.V., McMillen, W.T., Cai, S., Zhao, B., Whitesell, M., Shen, W., Kindler, L., Flack, R.S., Wu, W., Anderson, B., et al. (2020). ERK inhibitor LY3214996 targets ERK pathway-driven cancers: a therapeutic approach toward precision medicine. Mol. Cancer Ther. *19*, 325–336.

Björkdahl, O., Dohlsten, M., and Sjögren, H.O. (2000). Vaccination with B16 melanoma cells expressing a secreted form of interleukin-1beta induces tumor growth inhibition and an enhanced immunity against the wild-type B16 tumor. Cancer Gene Ther. *7*, 1365–1374.

Canli, Ö., Alankuş, Y.B., Grootjans, S., Vegi, N., Hültner, L., Hoppe, P.S., Schroeder, T., Vandenabeele, P., Bornkamm, G.W., and Greten, F.R. (2016). Glutathione peroxidase 4 prevents necroptosis in mouse erythroid precursors. Blood *127*, 139–148.

Chen, L., Hambright, W.S., Na, R., and Ran, Q. (2015). Ablation of the ferroptosis inhibitor glutathione peroxidase 4 in neurons results in rapid motor neuron degeneration and paralysis. J. Biol. Chem. *290*, 28097–28106.

Chu, B., Kon, N., Chen, D., Li, T., Liu, T., Jiang, L., Song, S., Tavana, O., and Gu, W. (2019). ALOX12 is required for p53-mediated tumour suppression through a distinct ferroptosis pathway. Nat. Cell Biol. *21*, 579–591.

Chung, Y., Chang, S.H., Martinez, G.J., Yang, X.O., Nurieva, R., Kang, H.S., Ma, L., Watowich, S.S., Jetten, A.M., Tian, Q., and Dong, C. (2009). Critical regulation of early Th17 cell differentiation by interleukin-1 signaling. Immunity *30*, 576–587.

Delgoffe, G.M., Woo, S.R., Turnis, M.E., Gravano, D.M., Guy, C., Overacre, A.E., Bettini, M.L., Vogel, P., Finkelstein, D., Bonnevier, J., et al. (2013). Stability and function of regulatory T cells is maintained by a neuropilin-1-semaphorin-4a axis. Nature *501*, 252–256.

Devos, D., Moreau, C., Devedjian, J.C., Kluza, J., Petrault, M., Laloux, C., Jonneaux, A., Ryckewaert, G., Garçon, G., Rouaix, N., et al. (2014). Targeting chelatable iron as a therapeutic modality in Parkinson's disease. Antioxid. Redox Signal. *21*, 195–210.

Dixon, S.J., Lemberg, K.M., Lamprecht, M.R., Skouta, R., Zaitsev, E.M., Gleason, C.E., Patel, D.N., Bauer, A.J., Cantley, A.M., Yang, W.S., et al. (2012). Ferroptosis: an iron-dependent form of nonapoptotic cell death. Cell *149*, 1060–1072.

Dobin, A., Davis, C.A., Schlesinger, F., Drenkow, J., Zaleski, C., Jha, S., Batut, P., Chaisson, M., and Gingeras, T.R. (2013). STAR: ultrafast universal RNA-seq aligner. Bioinformatics *29*, 15–21.

Doll, S., Proneth, B., Tyurina, Y.Y., Panzilius, E., Kobayashi, S., Ingold, I., Irmler, M., Beckers, J., Aichler, M., Walch, A., et al. (2017). ACSL4 dictates ferroptosis sensitivity by shaping cellular lipid composition. Nat. Chem. Biol. *13*, 91–98.

DuPage, M., and Bluestone, J.A. (2016). Harnessing the plasticity of CD4(+) T cells to treat immune-mediated disease. Nat. Rev. Immunol. *16*, 149–163.

Facciabene, A., Motz, G.T., and Coukos, G. (2012). T-regulatory cells: key players in tumor immune escape and angiogenesis. Cancer Res. *72*, 2162–2171.

Feng, H., Schorpp, K., Jin, J., Yozwiak, C.E., Hoffstrom, B.G., Decker, A.M., Rajbhandari, P., Stokes, M.E., Bender, H.G., Csuka, J.M., et al. (2020). Transferrin receptor is a specific ferroptosis marker. Cell Rep. *30*, 3411–3423.e7.

Field, C.S., Baixauli, F., Kyle, R.L., Puleston, D.J., Cameron, A.M., Sanin, D.E., Hippen, K.L., Loschi, M., Thangavelu, G., Corrado, M., et al. (2020). Mitochondrial integrity regulated by lipid metabolism is a cell-intrinsic checkpoint for Treg suppressive function. Cell Metab. *31*, 422–437.e5.

Fotaki, G., Jin, C., Ramachandran, M., Kerzeli, I.K., Karlsson-Parra, A., Yu, D., and Essand, M. (2017). Pro-inflammatory allogeneic DCs promote activation of bystander immune cells and thereby license antigen-specific T-cell responses. Oncoimmunology *7*, e1395126.

Frankish, A., Diekhans, M., Ferreira, A.M., Johnson, R., Jungreis, I., Loveland, J., Mudge, J.M., Sisu, C., Wright, J., Armstrong, J., et al. (2019). GENCODE reference annotation for the human and mouse genomes. Nucleic Acids Res. *47* (*D1*), D766–D773.

Gao, M., Monian, P., Quadri, N., Ramasamy, R., and Jiang, X. (2015). Glutaminolysis and transferrin regulate ferroptosis. Mol. Cell *59*, 298–308.

Gao, M., Yi, J., Zhu, J., Minikes, A.M., Monian, P., Thompson, C.B., and Jiang, X. (2019). Role of mitochondria in ferroptosis. Mol. Cell *73*, 354–363.e3.

Gerriets, V.A., Kishton, R.J., Nichols, A.G., Macintyre, A.N., Inoue, M., Ilkayeva, O., Winter, P.S., Liu, X., Priyadharshini, B., Slawinska, M.E., et al. (2015). Metabolic programming and PDHK1 control CD4$^+$ T cell subsets and inflammation. J. Clin. Invest. *125*, 194–207.

Hambright, W.S., Fonseca, R.S., Chen, L., Na, R., and Ran, Q. (2017). Ablation of ferroptosis regulator glutathione peroxidase 4 in forebrain neurons promotes cognitive impairment and neurodegeneration. Redox Biol. *12*, 8–17.

Josefowicz, S.Z., Lu, L.F., and Rudensky, A.Y. (2012). Regulatory T cells: mechanisms of differentiation and function. Annu. Rev. Immunol. *30*, 531–564.

Kagan, V.E., Mao, G., Qu, F., Angeli, J.P., Doll, S., Croix, C.S., Dar, H.H., Liu, B., Tyurin, V.A., Ritov, V.B., et al. (2017). Oxidized arachidonic and adrenic PEs navigate cells to ferroptosis. Nat. Chem. Biol. *13*, 81–90.

Kim, J.H., Lewin, T.M., and Coleman, R.A. (2001). Expression and characterization of recombinant rat acyl-CoA synthetases 1, 4, and 5. Selective inhibition by triacsin C and thiazolidinediones. J. Biol. Chem. *276*, 24667–24673.

Liu, Q., and Wang, K. (2019). The induction of ferroptosis by impairing STAT3/Nrf2/GPx4 signaling enhances the sensitivity of osteosarcoma cells to cisplatin. Cell Biol. Int. *43*, 1245–1256.

Liu, G., Yang, K., Burns, S., Shrestha, S., and Chi, H. (2010). The S1P(1)-mTOR axis directs the reciprocal differentiation of T(H)1 and T(reg) cells. Nat. Immunol. *11*, 1047–1056.

Love, M.I., Huber, W., and Anders, S. (2014). Moderated estimation of fold change and dispersion for RNA-seq data with DESeq2. Genome Biol. *15*, 550.

Lyssiotis, C.A., and Kimmelman, A.C. (2017). Metabolic interactions in the tumor microenvironment. Trends Cell Biol. *27*, 863–875.

Maj, T., Wang, W., Crespo, J., Zhang, H., Wang, W., Wei, S., Zhao, L., Vatan, L., Shao, I., Szeliga, W., et al. (2017). Oxidative stress controls regulatory T cell apoptosis and suppressor activity and PD-L1-blockade resistance in tumor. Nat. Immunol. *18*, 1332–1341.

Matsushita, M., Freigang, S., Schneider, C., Conrad, M., Bornkamm, G.W., and Kopf, M. (2015). T cell lipid peroxidation induces ferroptosis and prevents immunity to infection. J. Exp. Med. *212*, 555–568.

Michalek, R.D., Gerriets, V.A., Jacobs, S.R., Macintyre, A.N., MacIver, N.J., Mason, E.F., Sullivan, S.A., Nichols, A.G., and Rathmell, J.C. (2011). Cutting edge: distinct glycolytic and lipid oxidative metabolic programs are essential for effector and regulatory $CD4^+$ T cell subsets. J. Immunol. *186*, 3299–3303.

Mougiakakos, D., Johansson, C.C., and Kiessling, R. (2009). Naturally occurring regulatory T cells show reduced sensitivity toward oxidative stress-induced cell death. Blood *113*, 3542–3545.

Mougiakakos, D., Johansson, C.C., Jitschin, R., Böttcher, M., and Kiessling, R. (2011). Increased thioredoxin-1 production in human naturally occurring regulatory T cells confers enhanced tolerance to oxidative stress. Blood *117*, 857–861.

Newton, R., Priyadharshini, B., and Turka, L.A. (2016). Immunometabolism of regulatory T cells. Nat. Immunol. *17*, 618–625.

Nishikawa, H., and Sakaguchi, S. (2014). Regulatory T cells in cancer immunotherapy. Curr. Opin. Immunol. *27*, 1–7.

Overacre-Delgoffe, A.E., Chikina, M., Dadey, R.E., Yano, H., Brunazzi, E.A., Shayan, G., Horne, W., Moskovitz, J.M., Kolls, J.K., Sander, C., et al. (2017). Interferon-$\gamma$ drives $T_{reg}$ fragility to promote anti-tumor immunity. Cell *169*, 1130–1141.e11.

Pacella, I., Procaccini, C., Focaccetti, C., Miacci, S., Timperi, E., Faicchia, D., Severa, M., Rizzo, F., Coccia, E.M., Bonacina, F., et al. (2018). Fatty acid metabolism complements glycolysis in the selective regulatory T cell expansion during tumor growth. Proc. Natl. Acad. Sci. USA *115*, E6546–E6555.

Panduro, M., Benoist, C., and Mathis, D. (2016). Tissue Tregs. Annu. Rev. Immunol. *34*, 609–633.

Plitas, G., and Rudensky, A.Y. (2016). Regulatory T cells: differentiation and function. Cancer Immunol. Res. *4*, 721–725.

Proneth, B., and Conrad, M. (2019). Ferroptosis and necroinflammation, a yet poorly explored link. Cell Death Differ. *26*, 14–24.

Rubtsov, Y.P., Rasmussen, J.P., Chi, E.Y., Fontenot, J., Castelli, L., Ye, X., Treuting, P., Siewe, L., Roers, A., Henderson, W.R., Jr., et al. (2008). Regulatory T cell-derived interleukin-10 limits inflammation at environmental interfaces. Immunity *28*, 546–558.

Seiler, A., Schneider, M., Förster, H., Roth, S., Wirth, E.K., Culmsee, C., Plesnila, N., Kremmer, E., Rådmark, O., Wurst, W., et al. (2008). Glutathione peroxidase 4 senses and translates oxidative stress into 12/15-lipoxygenase dependent- and AIF-mediated cell death. Cell Metab. *8*, 237–248.

Sena, L.A., Li, S., Jairaman, A., Prakriya, M., Ezponda, T., Hildeman, D.A., Wang, C.R., Schumacker, P.T., Licht, J.D., Perlman, H., et al. (2013). Mitochondria are required for antigen-specific T cell activation through reactive oxygen species signaling. Immunity *38*, 225–236.

Smigiel, K.S., Richards, E., Srivastava, S., Thomas, K.R., Dudda, J.C., Klonowski, K.D., and Campbell, D.J. (2014). CCR7 provides localized access to IL-2 and defines homeostatically distinct regulatory T cell subsets. J. Exp. Med. *211*, 121–136.

Speiser, D.E., Ho, P.C., and Verdeil, G. (2016). Regulatory circuits of T cell function in cancer. Nat. Rev. Immunol. *16*, 599–611.

Stockwell, B.R., Friedmann Angeli, J.P., Bayir, H., Bush, A.I., Conrad, M., Dixon, S.J., Fulda, S., Gascón, S., Hatzios, S.K., Kagan, V.E., et al. (2017). Ferroptosis: a regulated cell death nexus linking metabolism, redox biology, and disease. Cell *171*, 273–285.

Togashi, Y., Shitara, K., and Nishikawa, H. (2019). Regulatory T cells in cancer immunosuppression—implications for anticancer therapy. Nat. Rev. Clin. Oncol. *16*, 356–371.

Van Den Eeckhout, B., Tavernier, J., and Gerlo, S. (2021). Interleukin-1 as innate mediator of T cell immunity. Front. Immunol. *11*, 621931.

Wang, W., Green, M., Choi, J.E., Gijón, M., Kennedy, P.D., Johnson, J.K., Liao, P., Lang, X., Kryczek, I., Sell, A., et al. (2019). $CD8^+$ T cells regulate tumour ferroptosis during cancer immunotherapy. Nature *569*, 270–274.

Wang, H., Franco, F., Tsui, Y.C., Xie, X., Trefny, M.P., Zappasodi, R., Mohmood, S.R., Fernández-García, J., Tsai, C.H., Schulze, I., et al. (2020). CD36-mediated metabolic adaptation supports regulatory T cell survival and function in tumors. Nat. Immunol. *21*, 298–308.

Weinberg, S.E., Singer, B.D., Steinert, E.M., Martinez, C.A., Mehta, M.M., Martínez-Reyes, I., Gao, P., Helmin, K.A., Abdala-Valencia, H., Sena, L.A., et al. (2019). Mitochondrial complex III is essential for suppressive function of regulatory T cells. Nature *565*, 495–499.

Yang, W.S., and Stockwell, B.R. (2008). Synthetic lethal screening identifies compounds activating iron-dependent, nonapoptotic cell death in oncogenic-RAS-harboring cancer cells. Chem. Biol. *15*, 234–245.

Yang, K., Neale, G., Green, D.R., He, W., and Chi, H. (2011). The tumor suppressor Tsc1 enforces quiescence of naive T cells to promote immune homeostasis and function. Nat. Immunol. *12*, 888–897.

Yang, W.S., SriRamaratnam, R., Welsch, M.E., Shimada, K., Skouta, R., Viswanathan, V.S., Cheah, J.H., Clemons, P.A., Shamji, A.F., Clish, C.B., et al. (2014). Regulation of ferroptotic cancer cell death by GPX4. Cell *156*, 317–331.

Yang, K., Blanco, D.B., Chen, X., Dash, P., Neale, G., Rosencrance, C., Easton, J., Chen, W., Cheng, C., Dhungana, Y., et al. (2018). Metabolic signaling directs the reciprocal lineage decisions of $\alpha\beta$ and $\gamma\delta$ T cells. Sci. Immunol. *3*, eaas9818.

Yoo, S.E., Chen, L., Na, R., Liu, Y., Rios, C., Van Remmen, H., Richardson, A., and Ran, Q. (2012). Gpx4 ablation in adult mice results in a lethal phenotype accompanied by neuronal loss in brain. Free Radic. Biol. Med. *52*, 1820–1827.

Yu, X., Lao, Y., Teng, X.L., Li, S., Zhou, Y., Wang, F., Guo, X., Deng, S., Chang, Y., Wu, X., et al. (2018). SENP3 maintains the stability and function of regulatory T cells via BACH2 deSUMOylation. Nat. Commun. *9*, 3157.

Zhivaki, D., Borriello, F., Chow, O.A., Doran, B., Fleming, I., Theisen, D.J., Pallis, P., Shalek, A.K., Sokol, C.L., Zanoni, I., and Kagan, J.C. (2020). Inflammasomes within hyperactive murine dendritic cells stimulate long-lived T cell-mediated anti-tumor immunity. Cell Rep. *33*, 108381.

## STAR★METHODS

### KEY RESOURCES TABLE

| REAGENT or RESOURCE | SOURCE | IDENTIFIER |
|---|---|---|
| Antibodies | | |
| Foxp3 (FJK-16 s) | Thermo Fisher Scientific | Cat#11-5773-82; RRID: AB_465243 |
| CD71 (RI7217) | BioLegend | Cat# 113807, RRID:AB_313568 |
| CD73 (TY/11.8) | BioLegend | Cat# 127206, RRID:AB_2154094 |
| IL-4 (11B11) | BioLegend | Cat# 504104, RRID:AB_315318 |
| CTLA4 (UC10-4B9) | BioLegend | Cat#106306; RRID: AB_313255 |
| LY6G (1A8) | BioLegend | Cat# 127607, RRID:AB_1186104 |
| NRP1(3E12) | BioLegend | Cat# 145206, RRID:AB_2562032 |
| TNFα (MP6-XT22) | BioLegend | Cat# 506307, RRID:AB_315428 |
| IFN-γ (XMG1.2) | BioLegend | Cat# 505810, RRID:AB_315404 |
| MHCII (M5/114.15.2) | BioLegend | Cat#107627; RRID: AB_1659252 |
| TCRβ (H57-597) | BioLegend | Cat#109220; RRID: AB_893624 |
| CD11C (N418) | BioLegend | Cat#117318; RRID: AB_493568 |
| CD62L (MEL-14) | BioLegend | Cat#104418; RRID: AB_313103 |
| PD1 (RMP1-30) | BioLegend | Cat#109109; RRID: AB_572016 |
| IL-17 (TC11-18H10.1) | BioLegend | Cat# 506921, RRID:AB_2125011 |
| CD4 (RM4-4) | BioLegend | Cat#116008; RRID: AB_11149680 |
| CD16/CD32 (2.4G2) | Tonbo | Cat#70-0161; RRID: AB_2621487 |
| CD8α (53-6.7) | BioLegend | Cat#100744; RRID: AB_2562609 |
| CD11b (M1/70) | BioLegend | Cat#101239; RRID: AB_11125575 |
| CD44 (IM7) | BioLegend | Cat#103049; RRID: AB_2562600 |
| ERK1/2 | CST | Cat# 4695; RRID: AB_390779 |
| Gpx4 | Abcam | Cat# ab125066, RRID:AB_10973901 |
| β-Actin (8H10D10) | CST | Cat#3700; RRID: AB_2242334 |
| Chemicals, peptides, and recombinant proteins | | |
| Liproxstatin-1 (Lip-1) | Caymanchem | Cat#17730; CAS: 950455-15-9 |
| α-Tocotrienol (α-Toc) | Caymanchem | Cat#10008377; CAS: 58864-81-6 |
| Pioglitazone (Pio) | Caymanchem | Cat#71745; CAS: Cat#111025-46-8 |
| Ferrostatin-1 (Fer-1) | Sigma-Aldrich | Cat#SML0583; CAS: 347174-05-4 |
| erastin | Fisher Scientific | Cat#NC1511737; CAS: 571203-78-6 |
| RSL3 | Fisher Scientific | Cat#NC1588949; CAS: 1219810-16-8 |
| BSO | Caymanchem | Cat#14484; CAS: 83730-53-4 |
| Deferiprone (DFP) | Caymanchem | Cat#28702; CAS: 1346601-82-8 |
| Ciclopirox (CPX) | Caymanchem | Cat#16021; CAS: 29342-05-0 |
| L-Glutathione reduced (GSH) | Sigma-Aldrich | Cat#G4251; CAS: 70-18-8 |
| LY3214996 | Selleck Chemicals | Cat# S8534; CAS: 1951483-29-6 |
| Necrostatin-1 (Nec-1) | Caymanchem | Cat#11658; CAS:4311-88-0 |
| Necrostatin 2 racemate (Nec-1 s) | Selleck Chemicals | Cat#S8641; CAS: 852391-15-2 |
| Z-VAD-FMK (Z-VAD) | Selleck Chemicals | Cat#S7023; CAS: 187389-52-2 |
| Caspase-1 Inhibitor (Casp1i) | R&D Systems | Cat# FMK002 |
| MitoTEMPO | Sigma-Aldrich | Cat# SML0737; CAS: 1334850-99-5 |
| BODIPY 581/591 C11 | Fisher Scientific | Cat#D3861; CAS: 217075-36-0 |
| Liperfluo | Dojindo | Cat#L248; CAS: 1448846-35-2 |

(*Continued on next page*)

*Continued*

| REAGENT or RESOURCE | SOURCE | IDENTIFIER |
|---|---|---|
| Ionomycin | Sigma-Aldrich | Cat#I9657; CAS: 56092-81-0 |
| Phorbol 12-myristate 13-acetate | Sigma-Aldrich | Cat#P8139; CAS: 16561-29-8 |
| BD GolgiStop | BD Biosciences | Cat#554724 |
| anti-mouse CD3ε antibody Clone 145-2C11 | Bio-X-Cell | Cat#BE0001-1 |
| anti-mouse CD28 antibody Clone 37.51 | Bio-X-Cell | Cat#BE0015-1 |
| Percoll | GE Healthcare | Cat#17-0891-01 |
| HBSS | GIBCO | Cat#14170161 |
| DPBS | GIBCO | Cat#14190144 |
| Click's Medium (EHAA) | IrvineScientific | Cat#9195 |
| Collagenase IV | Worthington Biochemical | Cat#LS004188 |
| DNase I | Sigma-Aldrich | Cat#D4263 |
| Interleukin 2 (human) | NCI | Cat#0136279328 |
| **Critical commercial assays** | | |
| MS column | Miltenyi | Cat#130-042-201 |
| Foxp3 / Transcription Factor Staining Buffer Set | Fisher Scientific | Cat#501129060 |
| ACK lysis buffer | Fisher Scientific | Cat#A1049201 |
| Naive CD4+ T Cell Isolation Kit, mouse | Miltenyi | Cat#130-104-453 |
| EasySep Mouse CD25 Regulatory T Cell Positive Selection Kit | Stemcell | Cat#18782 |
| Dynabeads Mouse $CD4^+CD25^+$ Treg Cells Kit | Fisher Scientific | Cat#11463D |
| mouse CD11C MicroBeads UltraPure | Miltenyi | Cat#130-108-338 |
| Cytofix fixation buffer | BD Biosciences | Cat#554655 |
| Cytofix wash buffer | BD Biosciences | Cat#554723 |
| Mouse IL-1 beta/IL-1F2 DuoSet ELISA | R&D Systems | Cat#DY401 |
| RNeasy Micro kit | QIAGEN | Cat#74004 |
| SuperScript III Reverse Transcriptase | Thermo Fisher Scientific | Cat#18080044 |
| **Deposited data** | | |
| RNA-sequencing | This paper | GEO: GSE160338 |
| **Experimental models: Cell lines** | | |
| Murine MC38 | H.B. Chi | St. Jude Children's Research Hospital |
| Murine B16.F10 | H.B. Chi | St. Jude Children's Research Hospital |
| **Experimental models: Organisms/strains** | | |
| Mouse: *Foxp3*$^{YFP\text{-}Cre}$ | A.Y. Rudensky | Memorial Sloan Kettering |
| Mouse: C57BL/6J | Stock No. 000664 | Jackson Laboratory |
| Mouse: C57BL/6J | Breeding core facility | Indiana University School of Medicine |
| Mouse: $Gpx4^{fl/fl}$ | Stock No: 027964 | Jackson Laboratory |
| Mouse: *Bcl2* transgenic | H.B. Chi | St. Jude Children's Research Hospital |
| **Oligonucleotides** | | |
| *Il1b* | Mm00434228_m1 | Thermo Fisher Scientific |
| *Gpx4* | Mm072995722_m1 | Thermo Fisher Scientific |
| *Actb* | Mm02619580_g1 | Thermo Fisher Scientific |
| Control siRNA | Cat#6201 | CST |
| ERK siRNA | Cat#sc-29308 | Santa Cruz Biotechnology |
| **Software and algorithms** | | |
| FlowJo (v10.6) | TreeStar | https://www.flowjo.com/ |
| Prism (v8) | GraphPad | https://www.graphpad.com/ |

## RESOURCE AVAILABILITY

### Lead contact

Further information and requests for resource/reagents should be directed to and will be fulfilled by the Lead Contact, Kai Yang (ky11@iu.edu)

### Materials availability

This study did not generate new unique reagents.

### Data and code availability

The RNA-seq datasets generated in this paper are available at NCBI GEO database (GSE160338).

## EXPERIMENTAL MODEL AND SUBJECT DETAILS

### Mouse strains

C57BL/6 mice and *Gpx4*$^{fl/fl}$ mice were purchased from the Jackson Laboratory or a breeding core facility at Indiana University School of Medicine. *Bcl2* transgenic mice have been described (Yang et al., 2011). *Foxp3*$^{YFP\text{-}Cre}$ (*Foxp3*$^{Cre}$) mice were gifts from A. Rudensky (Rubtsov et al., 2008). The age and gender-matched *Foxp3*$^{Cre}$*Gpx4*$^{fl/fl}$ mice and WT mice (*Foxp3*$^{Cre}$ males or *Foxp3*$^{Cre/Cre}$ females) as controls were used at 8-12-weeks old unless otherwise noted. All mice were kept in a specific pathogen-free facility in the Animal Resource Center at Indiana University School of Medicine, and all animal experiments were approved by the Institutional Animal Care and Use Committee.

### Subcutaneous implantation of murine MC38 or B16.F10 tumor cells

Murine MC38 colon adenocarcinoma cells and B16 melanoma cells were cultured in DMEM medium supplemented with 10% (vol/vol) FBS and 1% (vol/vol) penicillin–streptomycin. Gender- and age-matched WT and *Foxp3*$^{Cre}$*Gpx4*$^{fl/fl}$ mice were injected subcutaneously with $2 \times 10^5$ MC38 adenocarcinoma cells or $1.5 \times 10^5$ B16.F10 cells at the right flank. For Lip-1 administration, MC38 tumor-bearing mice were intraperitoneally injected with 30 mg/kg Lip-1 every day. Tumors were measured with digital calipers every other day. Tumor volumes were calculated by the formula: Length × Width × [(Length × Width) ^ 0.5] × $\pi$/6. To isolate tumor infiltrating lymphocytes (TILs), tumors were collected, minced and digested in RPMI buffer containing 2% FBS and collagenase IV (1 mg/ml) (Sigma Aldrich) at 37°C for 30 min. The digested tissues were filtered using nylon mesh. The cell suspension was centrifuged and separated by a 40%–70% Percoll density gradient (GE Healthcare). The cells layered between 40% and 70% fraction were collected and used for staining.

## METHOD DETAILS

### Flow cytometry

Single cell suspensions were incubated with the conjugated antibodies in PBS containing 2% (vol/vol) FBS. Ghost Dye™ Violet 510 (Tonbo) was used to stain dead cells. The following antibodies were used for surface staining: CD4 (RM4-4), CD8$\alpha$ (53-6.7), TCR$\beta$ (H57-597), CD44 (1M7), CD62L (MEL-14), CD71 (RI7217), CD73 (TY/11.8), LY6G (1A8), NRP1 (3E12), MHCII (M5/114.15.2), CD11C (N418), PD1 (RMP1-30), CD11b (M1/70). Antibodies used for intracellular proteins include: Foxp3 (FJK-16 s), CTLA4 (UC10-4B9), IFN-$\gamma$ (XMG1.2), IL-4 (11B11), TNF$\alpha$ (MP6-XT22), and IL-17 (TC11-18H10.1). All antibodies used in flow cytometry were purchased from Biolegend and Thermo Fisher Scientific if not otherwise indicated. CD16/CD32 was used for Fc receptor blocking antibody. To examine intracellular Gpx4, cells were stained with Gpx4 rabbit primary antibody at room temperature for 1.5 hours before staining with anti-rabbit secondary antibody at room temperature for 1.5 hours. For staining mitochondria, lymphocytes were incubated for 30 min at 37°C with 10 nM MitoTracker Deep Red (Life Technologies) or 20 nM TMRM (tetramethyl rhodamine, methyl ester; ImmunoChemistry Technologies) after staining surface markers. ROS were measured by incubation with 5 $\mu$M MitoSOX™ Red (Life Technologies) after staining surface markers. To examine lipid peroxidation, lymphocytes were incubated for 30 min at 37°C with 5 $\mu$M Liperfluo (Cat: L248; Dojindo) or 5 $\mu$M BODIPY 581/591 C11 (Cat: D3861; Fisher Scientific) after staining surface markers. To determine intracellular cytokines, T cells were stimulated for 4 h with PMA plus ionomycin in the presence of monensin before being stained according to the manufacturer's instructions (Thermo Fisher Scientific). Flow cytometry data were acquired on the Attune NxT flow cytometer (Invitrogen) and analyzed with Flowjo V10.6 (TreeStar).

### Cell purification and cultures

Purified Treg cells and naive CD4$^+$ T cells from spleens and peripheral lymph nodes were sorted on FACSAria sorter (BD Biosciences). DCs were enriched and sorted from spleen. Naive CD4$^+$ T cells, DCs, and Treg cells were cultured in Click's medium (plus $\beta$-mercaptoethanol) supplemented with 10% (vol/vol) FBS and 1% (vol/vol) penicillin–streptomycin. For cell activation, Treg cells were stimulated with plate-coated $\alpha$-CD3 (5 $\mu$g/ml; 2C11; Bio X Cell) and $\alpha$-CD28 (5 $\mu$g/ml; 37.51; Bio X Cell) in the presence or absence of IL-2 (200 U/ml) for the indicated time points.

### Cell death assay

Treg cells were purified or sorted from spleens and peripheral lymph nodes including inguinal, auxiliary and cervical lymph nodes using Dynabeads Regulatory $CD4^+/CD25^+$ T Cell Kit (Invitrogen). Purified or sorted Treg cells were stimulated with the plate-coated α-CD3-CD28 (5 μg/ml) and IL-2 (200 U/ml) with or without α-Tocotrienol (α-Toc, 10 μM), Ferrostatin-1 (Fer-1, 10 μM), Deferiprone (DFP, 70 μM), Ciclopirox (CPX, 1 μM), U0126 (10 μM), Pioglitazone (Pio, 20 μM), reduced L-Glutathione (GSH, 1 mM), liproxstatin-1 (Lip-1, 100 nM), necrostatin-1 (Nec-1, 10 μM), LY3214996 (5 μM), Nec-1 s (10 μM), Z-VAD-FMK (Z-VAD, 10 μM), Caspase-1 Inhibitor (Casp1i, 30 μM), or MitoTEMPO (100 μM) as indicated. RSL3 (10 μM), BSO (20 μM) or erastin (10 μM) were used to induce ferroptotic cell death of purified or sorted WT Treg cells. The percentage and number of live Treg cells (YFP positive) were determined by the Attune NxT flow cytometer.

### Immunoblot and quantitative RT-PCR

Immunoblots were performed as described previously (Yang et al., 2011), using the following antibodies: Gpx4 (Cat: ab125066; Abcam), ERK (Cat: 4695; Cell Signaling Technology), and β-Actin (Cat: 3700S; Cell Signaling Technology). RNA was extracted with microRNA isolation kit (QIAGEN), and RNA concentration was determined using a NanoDrop One spectrophotometer (Thermo Fisher Scientific). cDNA was synthesized with SuperScript III reverse transcriptase (Invitrogen). An ABI 7500 Real-time PCR system was used for quantitative PCR with the following probe sets from Applied Biosystems: *Il1b* (Mm00434228_m1), *Gpx4* (Mm072995722_m1), and *Actb* (Mm02619580_g1). Gene expression was normalized as n-fold difference to the housekeeping gene *Actb* as described (Liu et al., 2010).

### Coculture of naive $CD4^+$ T cells and DCs with the medium from activated Treg cells

Sorted Treg cells were stimulated with the plate-coated α-CD3-CD28 (5 μg/ml) and IL-2 (200 U/ml) in the presence or absence of Fer-1 (10 μM) for 1 day, and then spun down to harvest the supernatant for *in vitro* culture of naive $CD4^+$ T cells and DCs. Sorted DCs and purified naive $CD4^+$ T cells were seeded into 48 well-plate at ratio of 1 to 5 in the conditioned medium with addition of α-CD3 (2 μg/ml), α-CD28 (1 μg/ml), α-IL-2 (10 μg/ml), IL-6 (20 ng/ml), and IL-23 (10 ng/ml) in the presence or absence of IL-1β neutralizing antibody (10 μg/ml) for additional 5 days, followed by examination of IL-17 and IFN-γ production in $CD4^+$ T cells.

### siRNA transfection

Neon Transfection System was used to transfect Treg cells with control or ERK siRNA according to the manufacturer brochure. Briefly, sorted $2 \times 10^5$ of Treg cells were stimulated with α-CD3-CD28 for 48 h. Treg cells were washed with DPBS and resuspended Treg cells in buffer T containing control or ERK siRNA. Electroporation of Treg cells was executed under the condition of 1800 V/10 ms/2 pulses. Electroporated cells were immediately transferred into 48-well plate before RSL3 stimulation.

### Treg-mediated suppression of naive $CD4^+$ T cell proliferation

Naive $CD4^+$ T cells were purified from spleens and peripheral lymph nodes of CD45.1 mice, and labeled with 5 μM CellTrace in PBS at room temperature for 20 minutes. Sorted DCs and CellTrace-labeled naive $CD4^+$ T cells at ratio of 1 to 5 were cocultured with sorted Treg cells in the presence of 1 μg/ml α-CD3 with or without 10 μM Fer-1 for 3 days, followed by flow cytometry analysis of CellTrace dilution of $CD45.1^+CD4^+$ T cells.

## QUANTIFICATION AND STATISTICAL ANALYSIS

### RNA sequencing and library preparation

Treg cells enriched from the spleens and plns of WT and $Foxp3^{Cre}Gpx4^{fl/fl}$ mice (n = 3 each group) were sorted by a FACSAria II (BD). RNA was isolated from resting Treg cells or those stimulated with the plate-bound α-CD3-CD28 (5 μg/ml) for 4 h with the RNeasy Micro Kit (QIAGEN). Total RNA was first evaluated for its quantity, and quality, using Agilent Bioanalyzer 2100, and samples with an RNA integrity number of 8.5 or higher were used for library preparation. RNA (600 ng/ sample) was used to prepare single indexed strand specific cDNA library using TruSeq stranded mRNA library prep kit (Illumina). The library prep was assessed for quantity and size distribution using Qubit and Agilent 2100 Bioanalyzer. The pooled libraries were sequenced with 75bp single-end configuration on NextSeq500 (Illumina) using NextSeq 500/550 high output kit. The quality of sequencing was confirmed using a Phred quality score.

### RNA-sequencing data processing and analysis

The sequencing data consisted of 12 sets of paired-end RNA-seq files. These files were first evaluated individually using FastQC (Version 0.11.5). STAR (Version 2.7.3a) (Dobin et al., 2013) sequence aligner was used to align the sequencing reads to GRCm38 mouse reference (M25) genome (p6) from GENCODE (Frankish et al., 2019). RSEM (Version 1.3.0) (DuPage and Bluestone, 2016) was used to quantify the reads and summarize to the gene level. DESeq2 (Version 1.22.2) (Love et al., 2014) was used for the following DGE analysis. The Ensembl gene ID conversion to gene symbol was generated from the GTF file such that the Ensembl gene IDs each had a mapping to a gene symbol. For duplicate Ensembl gene IDs, the highest expression Ensembl gene ID was selected and assigned the gene symbol. Genes with no expression were removed. Differentially expressed genes were selected using absolute $\log_2$

fold change greater than 1.2 and FDR less than 0.05. The Ingenuity Pathway analysis (IPA, QIAGEN Inc., https://digitalinsights.qiagen.com/products-overview/discovery-insights-portfolio/analysis-and-visualization/qiagen-ipa/) was performed on DEGs with a cutoff value of 2-fold. The RNA-seq data can be accessed via NCBI GEO database (GSE160338).

### Statistical analysis

Data are presented as the mean ± SEM unless otherwise indicated. *P value*s were calculated by one-way ANOVA, two-way ANOVA, two-tailed unpaired Student's t test or two-tailed paired Student's t test using GraphPad Prism, unless otherwise noted. $p < 0.05$ (*), $p < 0.01$ (**), $p < 0.001$ (***) and $p < 0.0001$ (****) indicate statistically significant changes. *n* represents biological replicates. All the statistical details of experiments can be found in figure legends.